

Breaking the Dimensional Barrier: A Pontryagin-Guided Direct Policy Optimization for Continuous-Time Multi-Asset Portfolio

Jeonggyu Huh¹, Jaegi Jeon^{*2}, and Hyeng Keun Koo³

¹Department of Mathematics, Sungkyunkwan University, Republic of Korea

²Graduate School of Data Science, Chonnam National University, Republic of Korea

³Department of Financial Engineering, Ajou University, Republic of Korea

May 13, 2025

Abstract

Solving large-scale, continuous-time portfolio optimization problems involving numerous assets and state-dependent dynamics has long been challenged by the curse of dimensionality. Traditional dynamic programming and PDE-based methods, while rigorous, typically become computationally intractable beyond a few state variables ($\sim 3-6$ limit in prior studies). To overcome this critical barrier, we introduce the *Pontryagin-Guided Direct Policy Optimization* (PG-DPO) framework. PG-DPO leverages Pontryagin’s Maximum Principle (PMP) and backpropagation-through-time (BPTT) to directly inform neural network-based policy learning. A key contribution is our highly efficient *Projected PG-DPO* (*P-PGDPO*) variant. This approach uniquely utilizes BPTT to obtain rapidly stabilizing estimates of the Pontryagin costates and their crucial derivatives with respect to the state variables. These estimates are then analytically projected onto the manifold of optimal controls dictated by PMP’s first-order conditions, significantly reducing training overhead and enhancing accuracy. This enables a breakthrough in scalability: numerical experiments demonstrate that P-PGDPO successfully tackles problems with dimensions previously considered far out of reach (up to 50 assets and 10 state variables). Critically, the framework accurately captures complex intertemporal hedging demands, a feat often elusive for other methods in high-dimensional settings. P-PGDPO delivers near-optimal policies, offering a practical and powerful alternative for a broad class of high-dimensional continuous-time control problems.

1 Introduction

High-dimensional optimal control problems often fall prey to the “curse of dimensionality” (Bellman, 1966), whereby the computational cost of classical dynamic programming (DP) approaches grows exponentially with the number of state variables. In a continuous-time finance setting, this difficulty becomes starkly evident in multi-asset Merton problems (Merton, 1973), where an investor dynamically allocates wealth among numerous risky assets whose drift and volatility may depend on exogenous state variables such as macroeconomic indicators or stochastic volatility factors. While DP or Hamilton–Jacobi–Bellman (HJB) PDE solvers provide a rigorous framework for low-dimensional cases (Fleming and Soner, 2006; Bertsekas and Tsitsiklis, 1995), they become intractable as the number of assets or state dimensions increases. This difficulty is pervasive, impacting not only continuous-time settings (which are often addressed via discretization for numerical solution) but also analogous discrete-time models where similar state-space explosion issues arise. Consequently, prior influential studies in these domains are typically

*Corresponding Author: jaegijeon@jnu.ac.kr

limited to analyzing problems involving up to approximately 3-5 state variables (Campbell and Viceira, 1999; Lynch, 2001; Balduzzi and Lynch, 1999) or specific frameworks handling around 6 state variables (Garlappi and Skoulakis, 2010), often necessitating simulation-based approaches for tractability (Brandt et al., 2005).

A promising alternative is to employ *Pontryagin’s Maximum Principle (PMP)*, an indirect method that bypasses the explicit computation of value functions (Pontryagin, 2014; Yong and Zhou, 2012). Rather than storing or approximating a high-dimensional value grid, the PMP characterizes the optimal control in terms of forward-backward differential equations for the state and its *costate* (adjoint). Notably, adding one more state dimension does not produce an exponential explosion in computational requirements, in contrast to DP (Bellman, 1966; Campbell et al., 2003). This makes Pontryagin-based methods appealing for large-scale portfolio optimization problems involving many assets and exogenous state processes (Karatzas et al., 1987).

Recent advances in deep learning further enhance the scalability of methods for solving high-dimensional stochastic control problems (e.g., Han et al., 2018; Raissi et al., 2019, for general PDE-based approaches). Concurrently, deep learning techniques are being applied directly to financial dynamic programming and stochastic control. Some approaches tackle infinite horizon problems via the HJB equation (Duarte et al., 2024), or solve the HJB equation for utility maximisation under constraints using formulations based on second-order backward stochastic differential equations (2BSDEs) (Davey and Zheng, 2022). Others aim to directly solve associated nonlinear PDEs using methods like deep branching algorithms (Nguwi et al., 2024). While these BSDE-based methods and direct PDE solvers are powerful, applications such as the Merton HJB have revealed limitations in accuracy or efficiency for certain variants (Nguwi et al., 2024). Moreover, some works effectively leverage the Stochastic Maximum Principle (SMP) and adjoint BSDEs, often through duality methods, to handle even non-Markovian problems in finance (Davey and Zheng, 2022). Alongside these PDE-centric or BSDE-centric deep learning approaches, another line of research, more akin to reinforcement learning, focuses on directly parameterizing the control policy with neural networks and optimizing the expected objective function through simulation and gradient ascent (e.g., Zhang and Zhou, 2019; Kopeliovich and Pokojovy, 2024, for portfolio problems with transaction costs or under Heston dynamics). Our PMP-based PG-DPO framework builds upon similar ideas of direct policy optimization but is distinctively guided by the continuous-time optimality conditions of PMP. It utilizes BPTT-derived costate estimates for finite-horizon problems, aiming for enhanced scalability and a novel way to enforce optimality conditions for problems with sufficient regularity.

One notable strategy related to the use of adjoint methods in optimal control, and central to our work, is to *directly* parameterize the policy (i.e., consumption and investment controls) with neural networks, then apply backpropagation-through-time (BPTT) to enforce Pontryagin’s optimality conditions. This strategy, which we term the baseline “Pontryagin-Guided Direct Policy Optimization (PG-DPO),” circumvents the need to approximate value functions or PDE solutions. Instead, it uses simulation-based gradients that automatically incorporate the adjoint processes, drastically reducing computational overhead in high-dimensional settings (Kushner and Yin, 2003; Borkar and Borkar, 2008).

The purpose of this paper is to develop and implement this PG-DPO framework for the general *multi-asset, state-dependent* continuous-time portfolio problem. We consider an investor who must decide on a continuous consumption rate and an allocation to n risky assets with state-dependent drift and volatility. By parameterizing the policy with neural networks, we can capture potentially complex relationships dependent on both wealth and the exogenous state. We show how a single forward pass in simulation, coupled with a backward pass via automatic differentiation (BPTT), yields unbiased estimates of the costate processes that PMP requires, guiding the policy towards optimality without the drawbacks of DP. This approach fundamentally relies on the existence and accurate estimation of the costate processes dictated

by PMP, applicable whenever the control problem satisfies appropriate regularity conditions allowing for a well-defined Hamiltonian system.

Furthermore, we introduce the “**Projected PG-DPO**” (**P-PGDPO**) variant, which significantly enhances efficiency and accuracy. This variant exploits the observation that BPTT-derived costate estimates often stabilize much faster than the full policy network. Once the costates are sufficiently stable (after a short warm-up phase), one can *bypass* the potentially suboptimal neural policy outputs. Instead, these costate estimates are directly substituted into the PMP first-order conditions (FOCs), effectively *projecting* the learned costate information onto the manifold of controls satisfying PMP’s necessary conditions. This recovers a near-optimal control analytically at every time-state point with minimal additional training, significantly reducing computational burden. While other deep learning methods such as Deep BSDE are also applied to high-dimensional problems, their ability to accurately capture complex, state-dependent optimal policy structures, particularly the crucial intertemporal hedging components, has been limited in challenging financial applications. Our numerical experiments (Section 4) demonstrate that P-PGDPO not only scales to problems with **dozens of assets and state variables (e.g., $n=50$, $k=10$ in our experiments)** but, critically, it is capable of precisely disentangling and reproducing these vital hedging demands—a feat not typically achieved by existing approaches in such high-dimensional settings. To the best of our knowledge, this explicit and accurate recovery of complex hedging terms in a high-dimensional, PMP-guided direct policy optimization framework is a novel contribution. This superior performance in both scalability and fidelity to the true optimal policy, especially its nuanced components, highlights the transformative potential of leveraging the PMP structure via BPTT-derived costate estimates for tackling a broad class of complex, high-dimensional control problems where amenability to costate estimation under suitable regularity conditions exists.

The main contributions of this paper can be summarized as follows:

- We introduce Pontryagin-Guided Direct Policy Optimization (PG-DPO), and its highly efficient “Projected PG-DPO” (P-PGDPO) variant that uses PMP structure (specifically FOCs) and BPTT-derived costates to solve complex continuous-time control problems.
- We demonstrate through numerical experiments that P-PGDPO not only breaks the dimensional barrier in portfolio optimization (up to $n=50$ assets, $k=10$ factors), but critically, accurately captures complex intertemporal hedging demands in these high-dimensional settings, a capability not typically demonstrated by alternative deep learning approaches.

In the remainder of this paper, we first present the multi-asset Merton problem with exogenous states in Section 2. Section 3 introduces our Pontryagin-Guided Direct Policy Optimization (PG-DPO) algorithm, its Projected PG-DPO (P-PGDPO) extension, and provides a theoretical justification for the effectiveness of the P-PGDPO approach under specified regularity conditions. Numerical experiments presented in Section 4 confirm the framework’s scalability and near-optimal performance within this testbed, illustrating its potential for high-dimensional applications. Finally, Section 5 concludes and discusses potential future directions.

2 Multi-Asset Continuous-Time Portfolio Problem with State Variables

In this section, we present a multi-asset extension of Merton’s continuous-time portfolio problem (Merton, 1973; Kim and Omberg, 1996; Liu, 2007), allowing the investor to allocate wealth across multiple (potentially correlated) risky assets and a risk-free asset, while consuming continuously. Each risky asset features its own drift and volatility, leading to an n -dimensional *portfolio weight* vector $\boldsymbol{\pi}_t$. Furthermore, an exogenous *state process* $\mathbf{Y}_t \in \mathbb{R}^k$ influences market

parameters such as returns and interest rates, adding additional complexity to the investor's decision.

Although the wealth X_t remains scalar, the investor's optimal policy now depends on both $\boldsymbol{\pi}_t \in \mathbb{R}^n$ and a high-dimensional state \mathbf{Y}_t . We handle this through Pontryagin's maximum principle (Pontryagin, 2014; Yong and Zhou, 2012), introducing a costate for X_t and another for \mathbf{Y}_t . Numerically, one can represent $\{\boldsymbol{\pi}_t, C_t\}$ via neural networks, thereby enabling policy gradient or dynamic programming algorithms even in multi-asset, state-dependent environments.

2.1 Problem Formulation with State Variables and Neural Network Controls

Let $\mathbf{Y}_t \in \mathbb{R}^k$ be a vector of economic state variables that influence the distribution of asset returns. For instance, \mathbf{Y}_t could include interest rates, macroeconomic indices, volatility factors, etc. We assume each component $Y_{i,t}$ follows an Ito diffusion:

$$dY_{i,t} = \mu_{Y,i}(t, \mathbf{Y}_t) dt + \sigma_{Y,i}(t, \mathbf{Y}_t) dW_{i,t}^Y, \quad i = 1, \dots, k,$$

with $\text{Cov}(dW_{i,t}^Y, dW_{j,t}^Y) = \phi_{ij} dt$. In vector form,

$$d\mathbf{Y}_t = \boldsymbol{\mu}_Y(t, \mathbf{Y}_t) dt + \boldsymbol{\sigma}_Y(t, \mathbf{Y}_t) d\mathbf{W}_t^Y,$$

where $\boldsymbol{\mu}_Y(t, \mathbf{Y}_t)$ is the $k \times 1$ drift vector, $\boldsymbol{\sigma}_Y(t, \mathbf{Y}_t)$ is a $k \times k$ diagonal matrix of diffusion coefficients (i.e., $\boldsymbol{\sigma}_Y(t, \mathbf{Y}_t) = \text{diag}(\sigma_{Y,1}(t, \mathbf{Y}_t), \dots, \sigma_{Y,k}(t, \mathbf{Y}_t))$ where $\sigma_{Y,i}$ are the diffusion functions from the component-wise definition), and \mathbf{W}_t^Y is a k -dimensional Brownian motion whose components may be correlated.

We consider a financial market with n risky assets and one risk-free asset. The risk-free asset accumulates wealth at an instantaneous rate $r(t, \mathbf{Y}_t)$, which may depend on time and the current state. For $i = 1, \dots, n$, the price $S_{i,t}$ of the i -th risky asset follows

$$dS_{i,t} = S_{i,t}(\mu_i(t, \mathbf{Y}_t) dt + \sigma_i(t, \mathbf{Y}_t) dW_{i,t}^X).$$

Here, $\mu_i(t, \mathbf{Y}_t)$ is the instantaneous expected return and $\sigma_i(t, \mathbf{Y}_t)$ is the instantaneous volatility of asset i . The n scalar Brownian motions $W_{i,t}^X$ may be correlated amongst themselves ($\text{Cov}(dW_{i,t}^X, dW_{j,t}^X) = \psi_{ij} dt$) and with the state variable processes ($\text{Cov}(dW_{i,t}^X, dW_{j,t}^Y) = \rho_{ij} dt$). In vector notation, let $\boldsymbol{\mu}(t, \mathbf{Y}_t)$ be the $n \times 1$ vector of expected returns, $\boldsymbol{\sigma}(t, \mathbf{Y}_t)$ be the $n \times n$ diagonal matrix of volatilities, and \mathbf{W}_t^X be the $n \times 1$ vector of Brownian motions for the risky assets. The risky asset dynamics can be written compactly as

$$d\mathbf{S}_t = \text{diag}(\mathbf{S}_t) \boldsymbol{\mu}(t, \mathbf{Y}_t) dt + \text{diag}(\mathbf{S}_t) \boldsymbol{\sigma}(t, \mathbf{Y}_t) d\mathbf{W}_t^X.$$

Throughout, we work on a complete probability space $(\Omega, \mathcal{F}, \mathbb{P})$ that carries the $(n+k)$ -dimensional Brownian motion \mathbf{W}_t and its natural filtration $\{\mathcal{F}_t\}_{t \geq 0}$, augmented to satisfy the *usual conditions* (right-continuity and completeness).

The investor allocates wealth X_t between the risk-free asset and the n risky assets. Let $\boldsymbol{\pi}_t$ be the $n \times 1$ vector representing the fraction of wealth invested in each risky asset at time t . The investor also chooses a consumption rate C_t . The dynamics of the investor's wealth X_t are governed by the following stochastic differential equation (SDE):

$$dX_t = \left[X_t \left(r(t, \mathbf{Y}_t) + \boldsymbol{\pi}_t^\top (\boldsymbol{\mu}(t, \mathbf{Y}_t) - r(t, \mathbf{Y}_t) \mathbf{1}) \right) - C_t \right] dt + X_t \boldsymbol{\pi}_t^\top \boldsymbol{\sigma}(t, \mathbf{Y}_t) d\mathbf{W}_t^X. \quad (1)$$

Here, $\boldsymbol{\mu}(t, \mathbf{Y}_t) - r(t, \mathbf{Y}_t) \mathbf{1}$ represents the vector of instantaneous excess returns over the risk-free rate, and $\mathbf{1}$ is an $n \times 1$ vector of ones.

We impose regularity conditions on the market parameters.

Assumption 1 (Market-parameter regularity). *Fix a finite horizon $T > 0$. The coefficients defining the state process \mathbf{Y}_t and influencing the wealth dynamics X_t via Eq. (1), namely $\boldsymbol{\mu}_Y$, $\boldsymbol{\sigma}_Y$, $\boldsymbol{\mu}$, $\boldsymbol{\sigma}$, r , satisfy the following conditions.*

- (a) **Measurability and continuity.** *Each map is jointly Borel-measurable in (t, \mathbf{y}) and continuous in \mathbf{y} for every fixed $t \in [0, T]$.*
- (b) **Global Lipschitz continuity.** *There exists $K_{\text{Lip}} > 0$ such that for all $t \in [0, T]$ and $\mathbf{y}, \mathbf{y}' \in \mathbb{R}^k$,*

$$\begin{aligned} & \|\boldsymbol{\mu}_Y(t, \mathbf{y}) - \boldsymbol{\mu}_Y(t, \mathbf{y}')\| + \|\boldsymbol{\sigma}_Y(t, \mathbf{y}) - \boldsymbol{\sigma}_Y(t, \mathbf{y}')\| \\ & + \|\boldsymbol{\mu}(t, \mathbf{y}) - \boldsymbol{\mu}(t, \mathbf{y}')\| + \|\boldsymbol{\sigma}(t, \mathbf{y}) - \boldsymbol{\sigma}(t, \mathbf{y}')\| \leq K_{\text{Lip}} \|\mathbf{y} - \mathbf{y}'\|. \end{aligned}$$

- (c) **Linear growth.** *There exists $K_{\text{LG}} > 0$ such that for all $(t, \mathbf{y}) \in [0, T] \times \mathbb{R}^k$,*

$$\begin{aligned} & \|\boldsymbol{\mu}_Y(t, \mathbf{y})\|^2 + \|\boldsymbol{\sigma}_Y(t, \mathbf{y})\|^2 + \|\boldsymbol{\mu}(t, \mathbf{y})\|^2 + \|\boldsymbol{\sigma}(t, \mathbf{y})\|^2 \\ & \leq K_{\text{LG}}^2 (1 + \|\mathbf{y}\|^2), \quad |r(t, \mathbf{y})| \leq K_{\text{LG}} (1 + \|\mathbf{y}\|). \end{aligned}$$

Under Assumption 1, the SDE system for (\mathbf{Y}_t, X_t) (where X_t depends on the chosen controls $\boldsymbol{\pi}_t, C_t$) admits a unique strong solution for sufficiently well-behaved controls; see Oksendal (2013, Chs. 5-6) for details on existence and uniqueness theorems for SDEs.

The investor's objective is to choose an admissible control pair $(\boldsymbol{\pi}, C)$ that maximises the expected discounted utility

$$J(\boldsymbol{\pi}, C) = \mathbb{E} \left[\int_0^T e^{-\delta t} U(C_t) dt + \kappa e^{-\delta T} U(X_T) \right], \quad (2)$$

subject to the wealth dynamics (1) and the admissibility constraints stated later in Assumption 2. Here $\delta > 0$ is the subjective discount rate and $\kappa \geq 0$ weights the utility of terminal wealth (a bequest motive).

Throughout we work with the Hyperbolic Absolute Risk Aversion (HARA) family of utilities,

$$U(x) = \begin{cases} \frac{(a + bx)^{1-\gamma}}{1-\gamma}, & \gamma \neq 1, \\ \log(a + bx), & \gamma = 1, \end{cases} \quad b > 0, \gamma > 0, a \in \mathbb{R}, \quad (3)$$

whose domain is the half-line $\mathcal{D}_U := \{x > x_{\min}\}$ with $x_{\min} := -a/b$. HARA nests the familiar special cases CRRA ($a = 0, b = 1$) and CARA ($\gamma = 1, b = 1$). On its domain U is C^2 , strictly increasing and concave, and it satisfies the Inada limits $U'(x) \rightarrow \infty$ as $x \downarrow x_{\min}$ and $U'(x) \rightarrow 0$ as $x \rightarrow \infty$ (see Pennacchi, 2008, §3.2).

We restrict our attention to control processes that are economically sensible and mathematically tractable.

Assumption 2 (Admissible controls). *A control pair $(\boldsymbol{\pi}, C)$ is admissible if the following conditions hold:*

- (a) **Adaptedness.** *$(\boldsymbol{\pi}_t, C_t)_{0 \leq t \leq T}$ is $\{\mathcal{F}_t\}$ -progressively measurable, where $\{\mathcal{F}_t\}$ is the filtration generated by the underlying Brownian motions.*
- (b) **Integrability.**

$$\mathbb{E} \int_0^T (\|\boldsymbol{\pi}_t\|^2 + C_t) dt < \infty.$$

- (c) **Interior bounds.** *There exist constants $\Pi_{\max} > 0$ and $\xi \in (0, 1)$ such that*

$$\|\boldsymbol{\pi}_t\| < \Pi_{\max}, \quad 0 < C_t < \xi X_t, \quad \forall t \in [0, T] \text{ a.s.}$$

- (d) **Domain-admissible wealth.** With $x_{\min} := -a/b$ (see the HARA utility defined above) we require

$$X_t > x_{\min}, \quad \forall t \in [0, T] \text{ a.s.}$$

For clarity on the noise structure, we define the combined $(n+k)$ -dimensional Brownian vector $\mathbf{W}_t = (\mathbf{W}_t^{X\top}, \mathbf{W}_t^{Y\top})^\top$. The covariance structure of its increments $d\mathbf{W}_t$ is given by the matrix $\mathbf{\Omega}$:

$$\text{Cov}(d\mathbf{W}_t) = \mathbf{\Omega} dt = \begin{pmatrix} \Psi & \rho \\ \rho^\top & \Phi \end{pmatrix} dt,$$

where $\Psi = (\psi_{ij}) \in \mathbb{R}^{n \times n}$ is the covariance matrix of $d\mathbf{W}_t^X$, $\Phi = (\phi_{ij}) \in \mathbb{R}^{k \times k}$ is the covariance matrix of $d\mathbf{W}_t^Y$, and $\rho = (\rho_{ij}) \in \mathbb{R}^{n \times k}$ is the cross-covariance matrix.

Assumption 3 (Noise covariance). *The block covariance matrix $\mathbf{\Omega} = \begin{pmatrix} \Psi & \rho \\ \rho^\top & \Phi \end{pmatrix}$ is constant in time and uniformly positive definite: there exists $\lambda_\Omega > 0$ such that $z^\top \mathbf{\Omega} z \geq \lambda_\Omega \|z\|^2$ for all $z \in \mathbb{R}^{n+k}$. (Consequently, Ψ and Φ are individually positive definite and hence invertible.)*

Assumption 2(iii) gives the strict inequalities $0 < C_t < \xi X_t$, while Assumption 2(iv) guarantees the wealth process stays inside the utility's domain, $X_t > x_{\min} (= -a/b)$, almost surely. Since U is C^2 , strictly concave, and satisfies the Inada limits on (x_{\min}, ∞) , and because $\delta > 0$, we obtain

$$\mathbb{E} \left[e^{-\delta t} U(C_t) \right] \leq e^{-\delta t} U(\xi \mathbb{E}[X_t]) < \infty, \quad \mathbb{E}[U(X_T)] < \infty,$$

so the objective functional (2) is well defined for every admissible control pair $(\boldsymbol{\pi}, C)$.

The value function $V(t, x, \mathbf{y})$ associated with this problem represents the maximum expected utility achievable starting from wealth x and state \mathbf{y} at time t . Formally,

$$V(t, x, \mathbf{y}) = \sup_{(\boldsymbol{\pi}_s, C_s)_{s \in [t, T]}} \mathbb{E}_{t, x, \mathbf{y}} \left[\int_t^T e^{-\delta(s-t)} U(C_s) ds + \kappa e^{-\delta(T-t)} U(X_T) \right],$$

where the supremum is taken over all admissible control processes on $[t, T]$, and $\mathbb{E}_{t, x, \mathbf{y}}[\cdot] = \mathbb{E}[\cdot | X_t = x, \mathbf{Y}_t = \mathbf{y}]$ denotes the conditional expectation.

Assumption 4 (Uniform non-degeneracy and utility).

- (a) **Uniform non-degeneracy of risky-asset volatility.** Let $a(t, \mathbf{y}) := \boldsymbol{\sigma}(t, \mathbf{y}) \Psi \boldsymbol{\sigma}(t, \mathbf{y})^\top$. There exists $\lambda > 0$ such that

$$\mathbf{z}^\top a(t, \mathbf{y}) \mathbf{z} \geq \lambda \|\mathbf{z}\|^2, \quad \forall (t, \mathbf{y}, \mathbf{z}) \in [0, T] \times \mathbb{R}^k \times \mathbb{R}^n.$$

- (b) **Utility specification.** We use the HARA utility U in (3); on its domain $x > x_{\min}$ it is C^2 , strictly increasing ($U' > 0$), strictly concave ($U'' < 0$) and satisfies the Inada limits $U'(x) \rightarrow \infty$ as $x \downarrow x_{\min}$ and $U'(x) \rightarrow 0$ as $x \rightarrow \infty$.

- (c) **Discount and bequest parameters.** The subjective discount rate satisfies $\delta > 0$, and the terminal-wealth weight satisfies $\kappa \geq 0$.

Part (a) ensures the diffusion is non-degenerate, which guarantees parabolic regularity of the associated Hamilton–Jacobi–Bellman (HJB) equation. Part (b) specialises preferences to the HARA family; it reduces to CRRA when $a = 0$ (irrespective of b), and to the familiar log-utility when $a = 0$ and $\gamma = 1$. Together with the coefficient regularity of Assumption 1, these conditions yield existence, uniqueness, and sufficient smoothness of the value function (e.g. $V \in C^{1,2,2}$); see (Oksendal, 2013, Chs. 6–7).

In our numerical approach, we parameterize the control policies using neural networks (NNs). The portfolio allocation $\boldsymbol{\pi}_t$ and consumption rate C_t are represented as functions of the current time t , wealth X_t , and state \mathbf{Y}_t , determined by the NN parameters θ and ϕ :

$$\boldsymbol{\pi}_t = \boldsymbol{\pi}_\theta(t, X_t, \mathbf{Y}_t), \quad C_t = C_\phi(t, X_t, \mathbf{Y}_t).$$

These parameters θ and ϕ are then optimized to maximize the objective J .

2.2 Optimality Conditions via Pontryagin's Maximum Principle

We now apply Pontryagin's Maximum Principle (PMP) to the continuous-time portfolio problem formulated in Section 2.1, where market parameters depend on the exogenous state process $\{\mathbf{Y}_t\}_{0 \leq t \leq T}$. PMP provides necessary conditions for optimality through a system of forward-backward stochastic differential equations (FBSDEs), which couple the dynamics of the state variables with those of associated costate variables.

The system state includes the investor's wealth X_t and the exogenous state variables $\mathbf{Y}_t \in \mathbb{R}^k$. The corresponding costate processes represent the sensitivity of the value function V to changes in the state: $\lambda_t = V_x(t, X_t, \mathbf{Y}_t)$ is the scalar costate for wealth (marginal value of wealth), and $\boldsymbol{\eta}_t = V_{\mathbf{y}}(t, X_t, \mathbf{Y}_t)$ is the k -dimensional costate vector for the exogenous state variables (marginal value of state variables).

Under an optimal control policy $(\boldsymbol{\pi}_t^*, C_t^*)$, the evolution of the system state, comprising the wealth process X_t^* and the exogenous variables \mathbf{Y}_t , is described by the following forward stochastic differential equations:

$$dX_t^* = \left[X_t^* \left(r(t, \mathbf{Y}_t) + \boldsymbol{\pi}_t^{*\top} (\boldsymbol{\mu}(t, \mathbf{Y}_t) - r(t, \mathbf{Y}_t) \mathbf{1}) \right) - C_t^* \right] dt + X_t^* \boldsymbol{\pi}_t^{*\top} \boldsymbol{\sigma}(t, \mathbf{Y}_t) d\mathbf{W}_t^X, \quad (4)$$

$$d\mathbf{Y}_t = \boldsymbol{\mu}_Y(t, \mathbf{Y}_t) dt + \boldsymbol{\sigma}_Y(t, \mathbf{Y}_t) d\mathbf{W}_t^Y, \quad (5)$$

with initial conditions $X_0^* = x_0 > x_{\min}$ and $\mathbf{Y}_0 = \mathbf{y}_0 \in \mathbb{R}^k$. Recall the definitions of the volatility matrix $\boldsymbol{\sigma}(t, \mathbf{Y}_t)$ (for assets) and the covariance structure $\boldsymbol{\Omega}$ of the combined Brownian motion $\mathbf{W}_t = (\mathbf{W}_t^{X\top}, \mathbf{W}_t^{Y\top})^\top$.

Complementing these forward dynamics, the optimal costate processes $(\lambda_t^*, \boldsymbol{\eta}_t^*)$ satisfy a system of backward stochastic differential equations (BSDEs). These equations are driven by derivatives of the Hamiltonian \mathcal{H} associated with the control problem:

$$-d\lambda_t^* = \mathcal{H}_x(t, X_t^*, \mathbf{Y}_t, \boldsymbol{\pi}_t^*, C_t^*, \lambda_t^*, \boldsymbol{\eta}_t^*, \mathbf{Z}_t) dt - \mathbf{Z}_t^{\lambda X} d\mathbf{W}_t^X - \mathbf{Z}_t^{\lambda Y} d\mathbf{W}_t^Y, \quad (6)$$

$$-d\boldsymbol{\eta}_t^* = \mathcal{H}_{\mathbf{y}}(t, X_t^*, \mathbf{Y}_t, \boldsymbol{\pi}_t^*, C_t^*, \lambda_t^*, \boldsymbol{\eta}_t^*, \mathbf{Z}_t) dt - \mathbf{Z}_t^{\eta X} d\mathbf{W}_t^X - \mathbf{Z}_t^{\eta Y} d\mathbf{W}_t^Y. \quad (7)$$

Here, $\mathcal{H}_x = \partial \mathcal{H} / \partial x$ and $\mathcal{H}_{\mathbf{y}} = \nabla_{\mathbf{y}} \mathcal{H}$ represent the partial derivatives of the Hamiltonian. The terms $\mathbf{Z}_t^{\lambda X} \in \mathbb{R}^{1 \times n}$, $\mathbf{Z}_t^{\lambda Y} \in \mathbb{R}^{1 \times k}$, $\mathbf{Z}_t^{\eta X} \in \mathbb{R}^{k \times n}$, and $\mathbf{Z}_t^{\eta Y} \in \mathbb{R}^{k \times k}$ are adapted processes arising from the martingale representation theorem applied to the costates, collectively denoted by \mathbf{Z}_t . The derivatives $\mathcal{H}_x, \mathcal{H}_{\mathbf{y}}$ generally depend on the state, costate, controls, and the \mathbf{Z}_t terms themselves, reflecting the system's interconnectedness through the value function's second-order derivatives. The terminal conditions are determined by the objective functional: $\lambda_T^* = \kappa e^{-\delta T} U'(X_T^*)$ and $\boldsymbol{\eta}_T^* = \mathbf{0}$.

The application of PMP involves maximizing a Hamiltonian function. To properly account for the dependence of the wealth diffusion on the control $\boldsymbol{\pi}$, the Hamiltonian should incorporate the interaction between the costate dynamics (represented by \mathbf{Z} terms) and the diffusion coefficients. Following formulations in stochastic control theory (e.g., Yong and Zhou, 2012), the appropriate Hamiltonian \mathcal{H} can be expressed as:

$$\mathcal{H} = e^{-\delta t} U(C) + \lambda \left[x(r + \boldsymbol{\pi}^\top (\boldsymbol{\mu} - r\mathbf{1})) - C \right] + \boldsymbol{\eta}^\top \boldsymbol{\mu}_Y + \mathbf{Z}^{\lambda X} (x \boldsymbol{\sigma}^\top \boldsymbol{\pi}) + (\mathbf{Z}^{\eta X})^\top (x \boldsymbol{\sigma}^\top \boldsymbol{\pi}) + (\mathbf{Z}^{\eta Y})^\top \boldsymbol{\sigma}_Y. \quad (8)$$

For the $\boldsymbol{\pi}$ -FOC, only the drift term $\lambda x \boldsymbol{\pi}^\top (\boldsymbol{\mu}(t, \mathbf{Y}_t) - r(t, \mathbf{Y}_t) \mathbf{1})$ and the diffusion-coupling term $\mathbf{Z}^{\lambda X} (x \boldsymbol{\sigma}(t, \mathbf{Y}_t)^\top \boldsymbol{\pi})$ matter for the maximization step.

To ensure the well-posedness of this FBSDE system and the applicability of PMP, additional smoothness conditions on the model coefficients are typically required.

Assumption 5 (Additional regularity for PMP). *In addition to Assumptions 1, 2, and 4, we assume:*

- (a) *C^1 -regular coefficients w.r.t. \mathbf{y} . All coefficient functions $\boldsymbol{\mu}_Y, \boldsymbol{\sigma}_Y, \boldsymbol{\mu}, \boldsymbol{\sigma}, r$ are continuously differentiable with respect to the state vector \mathbf{y} . Furthermore, their partial derivatives $(\partial_{\mathbf{y}} f)$ are globally Lipschitz continuous in \mathbf{y} and satisfy linear growth conditions. This ensures that the drift terms in the costate BSDEs, involving derivatives like $\mathcal{H}_{\mathbf{y}}$, satisfy the required regularity conditions for the existence and uniqueness of solutions (cf. Yong and Zhou, 2012).*

The core requirement of Pontryagin's Maximum Principle is that the optimal controls $(\boldsymbol{\pi}_t^*, C_t^*)$ must maximize the Hamiltonian \mathcal{H} (8) pointwise in time, almost surely, given the optimal state and costate processes $(X_t^*, \mathbf{Y}_t, \lambda_t^*, \boldsymbol{\eta}_t^*, \mathbf{Z}_t^*)$. Assuming interior solutions allows us to derive the first-order conditions (FOCs) for optimality. Maximization with respect to the consumption rate C_t yields the standard condition:

$$e^{-\delta t} U'(C_t^*) = \lambda_t^*. \quad (9)$$

This classic result links optimal consumption $C_t^* = (U')^{-1}(e^{\delta t} \lambda_t^*)$ inversely to the marginal value of wealth λ_t^* . Maximization with respect to the portfolio weights $\boldsymbol{\pi}_t$ requires differentiating \mathcal{H} with respect to $\boldsymbol{\pi}$, including the term involving $\mathbf{Z}^{\lambda X}$. From (8), the relevant terms are $\lambda x \boldsymbol{\pi}^\top (\boldsymbol{\mu} - r \mathbf{1})$ and $\mathbf{Z}^{\lambda X} (x \boldsymbol{\sigma}^\top \boldsymbol{\pi})$. Setting the gradient $\nabla_{\boldsymbol{\pi}} \mathcal{H} = \mathbf{0}$ gives (assuming $X_t^* > 0$):

$$\lambda_t^* X_t^* (\boldsymbol{\mu}(t, \mathbf{Y}_t) - r(t, \mathbf{Y}_t) \mathbf{1}) + X_t^* \boldsymbol{\sigma}(t, \mathbf{Y}_t) (\mathbf{Z}_t^{\lambda X^*})^\top = \mathbf{0}.$$

Dividing by X_t^* , we obtain the FOC for the optimal portfolio:

$$\lambda_t^* (\boldsymbol{\mu}(t, \mathbf{Y}_t) - r(t, \mathbf{Y}_t) \mathbf{1}) + \boldsymbol{\sigma}(t, \mathbf{Y}_t) (\mathbf{Z}_t^{\lambda X^*})^\top = \mathbf{0}. \quad (10)$$

This first-order condition implicitly defines the optimal portfolio $\boldsymbol{\pi}_t^*$ through its dependence on the costate λ_t^* and the martingale component $\mathbf{Z}_t^{\lambda X^*}$.

To obtain an explicit expression for $\boldsymbol{\pi}_t^*$, we need to relate the martingale component $\mathbf{Z}^{\lambda X^*}$ to the derivatives of the value function. Applying Ito's lemma to $\lambda_t = V_x(t, X_t, \mathbf{Y}_t)$ and matching terms with the BSDE (6) establishes this relationship (the precise derivation often involves careful application of Ito's formula for processes driven by correlated Brownian motions, see e.g., standard texts or appendices like Appendix A). This procedure yields an expression for $\mathbf{Z}^{\lambda X^*}$ in terms of V_{xx}, V_{xy} , the optimal controls $\boldsymbol{\pi}_t^*$, and the model parameters $(\boldsymbol{\sigma}, \boldsymbol{\sigma}_Y, \Psi, \rho)$. Substituting this expression into the FOC (10) and solving the resulting algebraic equation for $\boldsymbol{\pi}_t^*$ leads to the well-known optimal portfolio formula:

$$\begin{aligned} \boldsymbol{\pi}_t^* = & -\frac{V_x}{X_t V_{xx}} \Sigma^{-1}(t, \mathbf{Y}_t) (\boldsymbol{\mu}(t, \mathbf{Y}_t) - r(t, \mathbf{Y}_t) \mathbf{1}) \\ & - \frac{1}{X_t V_{xx}} \Sigma^{-1}(t, \mathbf{Y}_t) (\boldsymbol{\sigma}(t, \mathbf{Y}_t) \boldsymbol{\rho} \boldsymbol{\sigma}_Y(t, \mathbf{Y}_t)) V_{xy}. \end{aligned} \quad (11)$$

Here, $\Sigma(t, \mathbf{Y}_t) = \boldsymbol{\sigma}(t, \mathbf{Y}_t) \Psi \boldsymbol{\sigma}(t, \mathbf{Y}_t)^\top$ represents the instantaneous covariance matrix of the risky asset returns. The value function derivatives $V_x = \lambda_t^*$, $V_{xx} = \partial_x \lambda_t^*$, and $V_{xy} = \nabla_{\mathbf{y}} \lambda_t^*$ (a $k \times 1$ vector) are evaluated along the optimal path (t, X_t^*, \mathbf{Y}_t) . The formula clearly separates the portfolio into two components: the *myopic demand*, which optimizes the immediate risk-return

trade-off as if the investment opportunity set were constant, and the *intertemporal hedging demand*, which adjusts the portfolio to mitigate risks arising from future stochastic changes in the state variables \mathbf{Y}_t . The hedging demand's magnitude and direction depend on the correlation ρ between asset returns and state variable innovations, and crucially on V_{xy} , which measures how the marginal value of wealth changes with the state variables.

For illustration, in the simplified case with one risky asset ($n = 1$) and one state variable ($k = 1$), the optimal allocation (11) becomes:

$$\pi_t^* = -\frac{V_x}{X_t V_{xx} \sigma^2} (\mu(t, Y_t) - r(t, Y_t)) - \frac{1}{X_t V_{xx} \sigma^2} (\sigma \rho \sigma_Y) V_{xy},$$

clearly showing the separation between the myopic component, proportional to the market price of risk, and the hedging component, proportional to V_{xy} and the correlation ρ .

2.3 Applications to Financial Models

2.3.1 A Multi-Asset Model with One OU Factor

We first consider a model with n risky assets whose risk premia are driven by a single Ornstein–Uhlenbeck (OU) factor. Specifically, each asset i has a constant volatility $\sigma_i > 0$ and a time-varying risk premium proportional to an OU state variable Y_t , such that the expected return is $r + \alpha_i \sigma_i Y_t$, where r is the constant risk-free rate. The state variable Y_t follows the OU process:

$$dY_t = \kappa_Y (\theta_Y - Y_t) dt + \sigma_Y dW_t^Y,$$

where $\kappa_Y > 0$ is the mean-reversion speed, $\theta_Y \in \mathbb{R}$ is the long-term mean, and $\sigma_Y > 0$ is the factor volatility. The Brownian motion W_t^Y may be correlated with the asset return processes.

The price dynamics for the i -th risky asset, $S_{i,t}$, are given by:

$$\frac{dS_{i,t}}{S_{i,t}} = (r + \alpha_i \sigma_i Y_t) dt + \sigma_i dW_{i,t}^S.$$

Let $\boldsymbol{\alpha} = (\alpha_1, \dots, \alpha_n)^\top$ be the vector of loading coefficients and $\boldsymbol{\sigma} = \text{diag}(\sigma_1, \dots, \sigma_n)$ be the diagonal matrix of constant asset volatilities, where each $\sigma_i > 0$. The Brownian motions driving the assets, $\mathbf{W}_t^S = (W_{1,t}^S, \dots, W_{n,t}^S)^\top$, have an $n \times n$ covariance matrix Ψdt , i.e., $\text{Cov}(d\mathbf{W}_t^S) = \Psi dt$. Furthermore, each $dW_{i,t}^S$ may have a correlation ρ_i with dW_t^Y ; let $\boldsymbol{\rho} = (\rho_1, \dots, \rho_n)^\top$.

Let X_t denote total wealth. The investor chooses a consumption rate $C_t \geq 0$ and portfolio weights $\boldsymbol{\pi}_t \in \mathbb{R}^n$ for the risky assets. The wealth dynamics follow:

$$dX_t = [X_t(r + \boldsymbol{\pi}_t^\top Y_t(\boldsymbol{\sigma}\boldsymbol{\alpha})) - C_t] dt + X_t \boldsymbol{\pi}_t^\top \boldsymbol{\sigma} d\mathbf{W}_t^S.$$

The instantaneous covariance matrix of the n -asset returns is $\Sigma = \boldsymbol{\sigma} \Psi \boldsymbol{\sigma}$.

For an investor with CRRA utility $U(x)$ and discount rate $\delta > 0$, the optimal consumption C_t^* is determined by $C_t^* = (U')^{-1}(e^{\delta t} \lambda_t^*)$, where λ_t^* is the costate associated with wealth X_t . The PMP first-order condition yields the optimal portfolio $\boldsymbol{\pi}_t^* \in \mathbb{R}^n$ as:

$$\boldsymbol{\pi}_t^* = -\frac{1}{X_t^* (\partial_x \lambda_t^*)} \Sigma^{-1} \{ \lambda_t^* Y_t (\boldsymbol{\sigma}\boldsymbol{\alpha}) + (\partial_Y \lambda_t^*) \sigma_Y (\boldsymbol{\sigma}\boldsymbol{\rho}) \}.$$

This expression involves the costate λ_t^* and its derivatives $\partial_x \lambda_t^*$ and $\partial_Y \lambda_t^*$. The first term within the braces represents the myopic demand driven by the risk premium $Y_t(\boldsymbol{\sigma}\boldsymbol{\alpha})$, and the second term captures the intertemporal hedging demand arising from the state variable Y_t . If $n = 1$, this simplifies to $\pi_t^* = -\frac{1}{\sigma^2 X_t^* \partial_x \lambda_t^*} \{ \lambda_t^* \alpha \sigma Y_t + \sigma (\partial_Y \lambda_t^*) \sigma_Y \rho \}$. For the specific case without intermediate consumption ($C_t = 0$), an analytic solution involving Riccati ODEs can be derived using the HJB framework (Kim and Omberg, 1996), as detailed in Appendix B.1.

2.3.2 A Multi-Asset, Multi-Factor Model

We then extend this setup to a more general *multi-factor* environment, considering n risky assets whose risk premia are driven by a k -dimensional OU factor vector $\mathbf{Y}_t \in \mathbb{R}^k$. The risk premium for asset $i = 1, \dots, n$ is $\sigma_i(\boldsymbol{\alpha}_i^\top \mathbf{Y}_t)$, where $\boldsymbol{\alpha}_i \in \mathbb{R}^k$ contains the factor loadings for asset i . The volatility σ_i for asset i is constant. This allows for richer interactions between multiple risk sources and asset returns.

The factor vector $\mathbf{Y}_t \in \mathbb{R}^k$ follows a multivariate OU process:

$$d\mathbf{Y}_t = \kappa_Y(\boldsymbol{\theta}_Y - \mathbf{Y}_t) dt + \boldsymbol{\sigma}_Y d\mathbf{W}_t^Y,$$

where $\kappa_Y \in \mathbb{R}^{k \times k}$ is a mean-reversion matrix, $\boldsymbol{\theta}_Y \in \mathbb{R}^k$ is the long-run mean vector, $\boldsymbol{\sigma}_Y$ is the $k \times k$ diagonal matrix of factor-specific diffusion coefficients (as defined in Section 2.1), and $d\mathbf{W}_t^Y$ is a k -dimensional vector of Brownian motions whose components may be correlated, with $\text{Cov}(d\mathbf{W}_t^Y) = \Phi dt$.

The n risky assets, with prices S_t^i , follow:

$$\frac{dS_t^i}{S_t^i} = \left(r + \sigma_i \boldsymbol{\alpha}_i^\top \mathbf{Y}_t \right) dt + \sigma_i dW_t^{X,i}, \quad i = 1, \dots, n.$$

Here, $\mathbf{W}_t^X \in \mathbb{R}^n$ is a Brownian motion with covariance matrix Ψdt . The asset shocks \mathbf{W}_t^X and factor shocks \mathbf{W}_t^Y can be correlated, with $\text{Cov}(dW_t^{X,i}, dW_t^{Y,j}) = \rho_{ij} dt$. Let $\boldsymbol{\rho} \in \mathbb{R}^{n \times k}$ be the matrix of cross-correlations.

With portfolio weights $\boldsymbol{\pi}_t = (\pi_t^1, \dots, \pi_t^n)^\top$ and consumption C_t , wealth X_t evolves as:

$$dX_t = \left[X_t \left(r + \sum_{i=1}^n \pi_t^i \sigma_i (\boldsymbol{\alpha}_i^\top \mathbf{Y}_t) \right) - C_t \right] dt + X_t \sum_{i=1}^n \pi_t^i \sigma_i dW_t^{X,i}.$$

For CRRA utility with discount δ , the optimal consumption C_t^* depends on the wealth costate λ_t^* . The optimal portfolio $\boldsymbol{\pi}_t^* \in \mathbb{R}^n$ is given by the PMP first-order condition (Eq. (11)), which in this context becomes:

$$\boldsymbol{\pi}_t^* = - \frac{1}{X_t^* (\partial_x \lambda_t^*)} \Sigma^{-1} \left\{ \lambda_t^* \boldsymbol{\sigma} \mathbf{A} \mathbf{Y}_t + \boldsymbol{\sigma} \boldsymbol{\rho} \boldsymbol{\sigma}_Y \partial_{\mathbf{Y}} \lambda_t^* \right\},$$

where $\boldsymbol{\sigma} = \text{diag}(\sigma_1, \dots, \sigma_n)$ is the $n \times n$ diagonal matrix of asset volatilities, $\Sigma = \boldsymbol{\sigma} \Psi \boldsymbol{\sigma}$ is the $n \times n$ asset return covariance, $\mathbf{A} = (\boldsymbol{\alpha}_1, \dots, \boldsymbol{\alpha}_n)^\top$ is the $n \times k$ matrix of factor loadings (where each $\boldsymbol{\alpha}_i$ is a $k \times 1$ vector of loadings for asset i), $\boldsymbol{\sigma}_Y$ is the $k \times k$ diagonal matrix of factor diffusion coefficients, and $\partial_{\mathbf{Y}} \lambda_t^*$ is the $k \times 1$ gradient vector of the costate with respect to the factors \mathbf{Y}_t . This explicitly separates the demand into a myopic part driven by the current expected excess returns ($\boldsymbol{\sigma} \mathbf{A} \mathbf{Y}_t$) and a hedging part driven by the sensitivity to factor changes ($\partial_{\mathbf{Y}} \lambda_t^*$) and their correlations ($\boldsymbol{\rho}, \Psi, \Phi$).

Similar to the single-factor case, an analytic solution for the terminal wealth problem ($C_t = 0$) with CRRA utility can often be found using an exponential-quadratic value function ansatz, leading to matrix Riccati ODEs. Details are presented in Appendix B.2.

3 A Gradient-Based Algorithm for Multi-Asset Policy Optimization

While Pontryagin's Maximum Principle (PMP) provides necessary optimality conditions via forward-backward stochastic differential equations (FBSDEs, Section 2.2), solving these analytically is often infeasible in high dimensions. We therefore adopt a *gradient-based* numerical approach using deep learning. The core idea is to parameterize the investor's policy $(\boldsymbol{\pi}_t, C_t)$ with neural networks $(\boldsymbol{\pi}_\theta(t, x, \mathbf{y}), C_\phi(t, x, \mathbf{y}))$, where (θ, ϕ) are the parameters to be optimized.

The objective is to find parameters (θ, ϕ) that maximize the expected utility achieved by the policy (π_θ, C_ϕ) . To ensure robustness across different starting scenarios, we aim to maximize the **extended value function**, $\tilde{J}(\theta, \phi)$. This is defined as the expected value of the conditional expected utility $J(t_0, x_0, \mathbf{y}_0; \theta, \phi)$ achieved under policy (θ, ϕ) , where the initial state (t_0, x_0, \mathbf{y}_0) is drawn from a distribution η over a relevant domain \mathcal{D} :

$$J(t_0, x_0, \mathbf{y}_0; \theta, \phi) = \mathbb{E}^{\theta, \phi} \left[\int_{t_0}^T e^{-\delta(u-t_0)} U(C_\phi(u, X_u, \mathbf{Y}_u)) du + \kappa e^{-\delta(T-t_0)} U(X_T) \middle| X_{t_0} = x_0, \mathbf{Y}_{t_0} = \mathbf{y}_0 \right] \quad (12)$$

$$\tilde{J}(\theta, \phi) = \mathbb{E}_{(t_0, x_0, \mathbf{y}_0) \sim \eta} [J(t_0, x_0, \mathbf{y}_0; \theta, \phi)] \quad (13)$$

Here, $\mathbb{E}^{\theta, \phi}[\cdot]$ denotes expectation under the dynamics generated by policy (θ, ϕ) .

This paper develops and implements the *Pontryagin-Guided Direct Policy Optimization* (PG-DPO) framework to maximize $\tilde{J}(\theta, \phi)$. PG-DPO leverages automatic differentiation, specifically backpropagation-through-time (BPTT), applied to Monte Carlo simulations drawn from the initial state distribution η . A key feature is that BPTT applied to these simulations yields not only unbiased estimates of the policy gradient $\nabla \tilde{J}$ needed for optimization, but also inherently calculates estimates of the Pontryagin costate variables $(\lambda_k^{(i)}, \boldsymbol{\eta}_k^{(i)})$ along each path, representing sensitivities dictated by PMP.

This dual output enables distinct algorithmic approaches: the baseline PG-DPO method is detailed in Section 3.1, and the advanced ‘‘Two-Stage PG-DPO’’ variant, which leverages these costate estimates more directly, is explored in Section 3.2.

3.1 Baseline PG-DPO for the Extended Objective

The baseline PG-DPO algorithm aims to maximize the extended value function $\tilde{J}(\theta, \phi)$ (defined in Eq. (13)) using mini-batch stochastic gradient ascent. The core idea is to approximate the gradient $\nabla \tilde{J}$ by averaging gradients computed on individual sample paths, where each path starts from a randomly drawn initial state. Each iteration j of the algorithm involves the following steps:

1. **Sample Initial States:** Draw a mini-batch of M initial states $\{(t_0^{(i)}, x_0^{(i)}, \mathbf{y}_0^{(i)})\}_{i=1}^M$ from the distribution η over the domain \mathcal{D} .
2. **Simulate Forward Paths:** For each sampled initial state i , simulate a discrete-time trajectory $\{(X_k^{(i)}, \mathbf{Y}_k^{(i)})\}_{k=0}^N$ forward from $t_k = t_0^{(i)}$ to $t_N = T$, using the current policy networks (π_θ, C_ϕ) . The state evolution follows:

$$\begin{aligned} \mathbf{Y}_{k+1}^{(i)} &= \mathbf{Y}_k^{(i)} + \boldsymbol{\mu}_Y(t_k^{(i)}, \mathbf{Y}_k^{(i)}) \Delta t^{(i)} + \boldsymbol{\sigma}_Y(t_k^{(i)}, \mathbf{Y}_k^{(i)}) \Delta \mathbf{W}_k^{(i), Y}, \\ X_{k+1}^{(i)} &= X_k^{(i)} + \left[X_k^{(i)} \left((1 - \boldsymbol{\pi}_k^{(i)\top} \mathbf{1}) r(t_k^{(i)}, \mathbf{Y}_k^{(i)}) + \boldsymbol{\pi}_k^{(i)\top} \boldsymbol{\mu}(t_k^{(i)}, \mathbf{Y}_k^{(i)}) \right) - C_k^{(i)} \right] \Delta t^{(i)} \\ &\quad + X_k^{(i)} \boldsymbol{\pi}_k^{(i)\top} \boldsymbol{\sigma}(t_k^{(i)}, \mathbf{Y}_k^{(i)}) \Delta \mathbf{W}_k^{(i), X}, \end{aligned}$$

where $\Delta t^{(i)} = (T - t_0^{(i)})/N$, $\boldsymbol{\sigma}_Y(t_k^{(i)}, \mathbf{Y}_k^{(i)})$ is the vector of diffusion coefficients applied element-wise to the components of $\Delta \mathbf{W}_k^{(i), Y}$, and the correctly correlated Brownian increments $(\Delta \mathbf{W}_k^{(i), X}, \Delta \mathbf{W}_k^{(i), Y})$ are derived from the Cholesky factor L of the overall covariance matrix $\boldsymbol{\Omega}$.

3. **Calculate Realized Reward per Path:** For each path i , compute the realized cumulative reward, explicitly noting its dependence on the starting state and policy parameters, denoted as $J^{(i)}(t_0^{(i)}, x_0^{(i)}, \mathbf{y}_0^{(i)}; \theta, \phi)$:

$$J^{(i)}(t_0^{(i)}, x_0^{(i)}, \mathbf{y}_0^{(i)}; \theta, \phi) = \sum_{k=0}^{N-1} e^{-\delta(t_k^{(i)} - t_0^{(i)})} U(C_\phi(t_k^{(i)}, X_k^{(i)}, \mathbf{Y}_k^{(i)})) \Delta t^{(i)} + \kappa e^{-\delta(T - t_0^{(i)})} U(X_N^{(i)}).$$

This value $J^{(i)}(t_0^{(i)}, \dots)$ is a stochastic sample related to the conditional expected utility $J(t_0^{(i)}, \dots)$ defined in Eq. (12).

4. **Apply BPTT for Policy Gradient Estimate:** Treat the simulation process for path i as a computational graph. Apply automatic differentiation (BPTT) to compute the gradient of the realized reward $J^{(i)}(t_0^{(i)}, \dots)$ with respect to the policy parameters (θ, ϕ) :

$$\nabla_{(\theta, \phi)} J^{(i)}(t_0^{(i)}, x_0^{(i)}, \mathbf{y}_0^{(i)}; \theta, \phi).$$

This gradient serves as an unbiased estimate related to the gradient of the conditional expected utility $J(t_0^{(i)}, \dots)$.

5. **Estimate Gradient of \tilde{J} :** Obtain an unbiased estimate for the gradient of the overall extended objective \tilde{J} by averaging the individual path gradients over the mini-batch:

$$\nabla \tilde{J}(\theta, \phi) \approx \nabla_{\text{batch}} = \frac{1}{M} \sum_{i=1}^M \nabla_{(\theta, \phi)} J^{(i)}(t_0^{(i)}, x_0^{(i)}, \mathbf{y}_0^{(i)}; \theta, \phi).$$

6. **Update Policy Parameters:** Update the parameters (θ, ϕ) using this averaged gradient estimate via stochastic gradient ascent:

$$(\theta, \phi)_{j+1} \leftarrow (\theta, \phi)_j + \alpha_j \nabla_{\text{batch}},$$

where α_j is the learning rate.

By iterating these steps, the baseline PG-DPO algorithm gradually optimizes the policy $(\boldsymbol{\pi}_\theta, C_\phi)$ to maximize the extended value function \tilde{J} .

Role of Intermediate BPTT Values and the ‘‘Pontryagin-Guided’’ Nature. It is important to understand the role of the intermediate values computed during BPTT in Step 4. As BPTT calculates the policy gradient $\nabla_{(\theta, \phi)} J^{(i)}(\dots)$ via the chain rule, it inherently computes the partial derivatives of the realized reward $J^{(i)}(\dots)$ with respect to the intermediate states along path i :

$$\lambda_k^{(i)} = \frac{\partial J^{(i)}(t_0^{(i)}, \dots)}{\partial X_k^{(i)}}, \quad \boldsymbol{\eta}_k^{(i)} = \frac{\partial J^{(i)}(t_0^{(i)}, \dots)}{\partial \mathbf{Y}_k^{(i)}}.$$

These sensitivities, computed mechanically by AD, are directly linked to the discrete adjoint Backward Stochastic Differential Equation (BSDE) structure required by Pontryagin’s Maximum Principle (PMP). To illustrate this crucial connection for the wealth component (denoting $\lambda_k^{(i)}$ for $\lambda_k^{X, (i)}$ for simplicity), consider the discrete Euler-Maruyama step for wealth under policy $(\boldsymbol{\pi}_k^{(i)}, C_k^{(i)})$:

$$X_{k+1}^{(i)} = X_k^{(i)} + \left[X_k^{(i)} \left(r(t_k, \mathbf{Y}_k^{(i)}) + \boldsymbol{\pi}_k^{(i)\top} (\boldsymbol{\mu}(t_k, \mathbf{Y}_k^{(i)}) - r(t_k, \mathbf{Y}_k^{(i)}) \mathbf{1}) \right) - C_k^{(i)} \right] \Delta t + X_k^{(i)} \boldsymbol{\pi}_k^{(i)\top} \boldsymbol{\sigma}(t_k, \mathbf{Y}_k^{(i)}) \Delta \mathbf{W}_k^{(i)}.$$

Algorithm 1 Baseline Pontryagin-Guided Direct Policy Optimization (PG-DPO)

Inputs:

Require: Policy nets π_θ, C_ϕ ; learning-rate schedule $\{\alpha_j\}_{j=0}^{J_{\max}-1}$; max iters J_{\max} , batch size M , time steps N ; initial-state distribution η ; utility U , discount δ , terminal weight κ ; market params $(\boldsymbol{\mu}, \boldsymbol{\sigma}, r, \boldsymbol{\mu}_Y, \boldsymbol{\sigma}_Y$ (k-dim vector of diff. coeffs.), $\boldsymbol{\Omega}$)

Output: optimised params $(\theta_{\text{opt}}, \phi_{\text{opt}})$

```

1: Initialise  $\theta, \phi$ 
2: for  $j = 0$  to  $J_{\max} - 1$  do
3:   Draw mini-batch  $\{(t_0^{(i)}, x_0^{(i)}, \mathbf{y}_0^{(i)})\}_{i=1}^M \sim \eta$ 
4:    $\nabla_{\text{batch}} \leftarrow \mathbf{0}$ 
5:   for  $i = 1$  to  $M$  do
6:      $(X_0, \mathbf{Y}_0) \leftarrow (x_0^{(i)}, \mathbf{y}_0^{(i)})$ ,  $\Delta t \leftarrow (T - t_0^{(i)})/N$ 
7:     for  $k = 0$  to  $N - 1$  do
8:        $t_k \leftarrow t_0^{(i)} + k\Delta t$ 
9:        $\boldsymbol{\pi}_k \leftarrow \pi_\theta(t_k, X_k, \mathbf{Y}_k)$ 
10:       $C_k \leftarrow C_\phi(t_k, X_k, \mathbf{Y}_k)$ 
11:      Sample  $\Delta \mathbf{W}_k \sim \mathcal{N}(\mathbf{0}, \boldsymbol{\Omega}\Delta t)$ 
12:       $\mathbf{Y}_{k+1} = \mathbf{Y}_k + \boldsymbol{\mu}_Y(t_k, \mathbf{Y}_k)\Delta t + \boldsymbol{\sigma}_Y(t_k, \mathbf{Y}_k) \Delta \mathbf{W}_k^Y$ 
13:       $X_{k+1} = X_k + \left[ X_k(r(t_k, \mathbf{Y}_k) + \boldsymbol{\pi}_k^\top(\boldsymbol{\mu}(t_k, \mathbf{Y}_k) - r(t_k, \mathbf{Y}_k)\mathbf{1})) - C_k \right] \Delta t + X_k \boldsymbol{\pi}_k^\top \boldsymbol{\sigma}(t_k, \mathbf{Y}_k) \Delta \mathbf{W}_k^X$ 
14:    end for
15:     $J^{(i)} = \sum_{k=0}^{N-1} e^{-\delta(t_k - t_0^{(i)})} U(C_k)\Delta t + \kappa e^{-\delta(T - t_0^{(i)})} U(X_N)$ 
16:     $g^{(i)} \leftarrow \nabla_{(\theta, \phi)} J^{(i)}$ 
17:     $\nabla_{\text{batch}} \leftarrow \nabla_{\text{batch}} + g^{(i)}$ 
18:  end for
19:   $(\theta, \phi) \leftarrow (\theta, \phi) + \frac{\alpha^j}{M} \nabla_{\text{batch}}$ 
20: end for
21: return  $(\theta, \phi)$ 

```

Applying the chain rule one step backward ($\lambda_k^{(i)} = \lambda_{k+1}^{(i)} \frac{\partial X_{k+1}^{(i)}}{\partial X_k^{(i)}}$) and using a first-order expansion yields the following backward recurrence relation along the path (i) (this illustrative recurrence primarily shows influences from the wealth dynamics; a full derivation of the drift for $\lambda_k^{(i)}$ from the total reward $J^{(i)}$ would also account for terms related to consumption $U(C_k^{(i)})$ and the discount factor in its definition within the Hamiltonian context):

$$\lambda_k^{(i)} \approx \lambda_{k+1}^{(i)} + \lambda_{k+1}^{(i)} [r + \pi_k^{(i)}(\mu - r)] \Delta t + \lambda_{k+1}^{(i)} \pi_k^{(i)} \boldsymbol{\sigma} \Delta \mathbf{W}_k^{(i)}.$$

This equation inherently possesses the structure of a discrete BSDE operating along the specific simulation path (i) . To formally connect this to the BSDE formulation in PMP, which involves processes adapted to the filtration $\{\mathcal{F}_{t_k}\}$ (representing available information at time t_k), one defines the adapted costate $\lambda_k = \mathbb{E}[\lambda_k^{(i)} | \mathcal{F}_{t_k}]$ and the predictable martingale component Z_k (related to the conditional expectation of $\lambda_{k+1}^{(i)} \Delta \mathbf{W}_k^{(i)}$). Taking the conditional expectation ($\mathbb{E}[\cdot | \mathcal{F}_{t_k}]$) of a more complete pathwise recurrence relation (inclusive of all terms affecting $J^{(i)}$) and carefully defining Z_k using a covariation-based approach, leads precisely to the standard discrete BSDE for the adapted process λ_k :

$$\lambda_k = \lambda_{k+1} + \underbrace{(\lambda_{k+1}[r + \pi_k(\mu - r)] + \pi_k \boldsymbol{\sigma} Z_k)}_{\approx \partial_x \mathcal{H}(t_k, \dots) \text{ from PMP}} \Delta t - Z_k \Delta \mathbf{W}_k. \quad (14)$$

Crucially, the drift term derived through this process corresponds exactly to the derivative of the discrete-time Hamiltonian ($\partial_x \mathcal{H}$) from PMP with respect to the state variable x . A similar structure holds for the costate vector $\boldsymbol{\eta}_k$ associated with the state variables \mathbf{Y}_k .

Therefore, the values $\lambda_k^{(i)}$ and $\boldsymbol{\eta}_k^{(i)}$ computed by BPTT are indeed pathwise numerical counterparts related to the Pontryagin costates, satisfying the relevant discrete BSDE structure. Crucially, in the *baseline* PG-DPO algorithm, these costate estimates themselves (and their potential derivatives w.r.t. states) are **not directly used** in the parameter update rule (Step 6), which only requires the final gradient $\nabla_{(\theta,\phi)} J^{(i)}(\dots)$.

Nevertheless, the fact that BPTT provides access to these theoretically grounded estimates is fundamental. Firstly, they are essential inputs for the **Projected PGDPO** variant discussed in the next subsection (§3.2). The baseline algorithm thus lays the groundwork by generating these estimates. Secondly, this deep connection explains why the algorithm is termed **Pontryagin-Guided**. Even though the baseline update only uses $\nabla_{(\theta,\phi)} J^{(i)}(\dots)$, the calculation of this gradient via BPTT structurally mirrors the backward propagation of sensitivities inherent in PMP’s adjoint equations (BSDEs), using the costate estimates $\lambda_k^{(i)}, \boldsymbol{\eta}_k^{(i)}$ implicitly within the chain rule (cf. Huh, 2024). Consequently, the optimization process, driven by these BPTT-computed gradients, is implicitly guided by the optimality conditions derived from Pontryagin’s principle, aiming to maximize the expected objective \tilde{J} .

3.2 Projected PG-DPO (P-PGDPO) Algorithm

While the baseline PG-DPO algorithm described in Section 3.1 effectively optimizes the extended objective \tilde{J} by training the policy networks $(\boldsymbol{\pi}_\theta, C_\phi)$ end-to-end, it can sometimes require a significant number of iterations for the networks to fully converge. The Projected PG-DPO (P-PGDPO) variant offers a potentially more computationally efficient alternative by exploiting an empirical observation: the costate estimates $(\lambda_k^{(i)}, \boldsymbol{\eta}_k^{(i)})$ and their relevant derivatives with respect to states, like $\partial_x \lambda_k^{(i)}, \partial_{\mathbf{Y}} \lambda_k^{(i)}$, which are generated during BPTT, often stabilize and become reasonably accurate much faster than the full policy networks achieve optimality. This P-PGDPO approach leverages these rapidly stabilizing costate estimates to construct near-optimal controls directly by projecting them onto the manifold of policies satisfying the PMP first-order conditions.

This P-PGDPO approach leverages these rapidly stabilizing costate estimates to construct near-optimal controls directly from the PMP first-order conditions, bypassing the need for fully converged policy networks for deployment. The procedure consists of two distinct stages, described below using a single level of enumeration:

1. Stage 1: Warm-Up Phase for Costate Estimation

First, we execute the **Baseline PG-DPO process**, as detailed in Section 3.1 (which optimizes \tilde{J}), for a predetermined, relatively small number of iterations, K_0 . The primary objective of this stage is **not** to obtain fully optimized networks $(\boldsymbol{\pi}_\theta, C_\phi)$, but rather to run the BPTT process sufficiently long for the underlying mechanism generating the **costate estimates** $(\lambda_k^{(i)} = \partial J^{(i)}(\dots)/\partial X_k^{(i)}, \boldsymbol{\eta}_k^{(i)} = \partial J^{(i)}(\dots)/\partial \mathbf{Y}_k^{(i)})$ and their relevant state-derivatives (e.g., $\partial_x \lambda_k^{(i)}, \partial_{\mathbf{Y}} \lambda_k^{(i)}$) to stabilize. We let (θ^*, ϕ^*) denote the policy parameters obtained at the end of this warm-up phase.

2. Stage 2: Analytic Control Deployment

After completing the K_0 warm-up iterations, the trained policy networks $(\boldsymbol{\pi}_{\theta^*}, C_{\phi^*})$ are typically **not directly used** for generating controls during deployment. Instead, to determine the control actions for any given state (t_k, X_k, \mathbf{Y}_k) encountered during deployment (let this deployment time be $t_k = t_{\text{deploy}}$), we employ a Monte Carlo-like averaging procedure to obtain reliable costate estimates needed for the PMP formulas:

First, to obtain the **stabilized costate estimates** corresponding to the state $(t_{\text{deploy}}, X_k, \mathbf{Y}_k)$, we perform the following averaging: Simulate multiple (M_{MC}) forward paths starting from $(t_{\text{deploy}}, X_k, \mathbf{Y}_k)$ (or states very close to it) up to the horizon T , using the *fixed* policy

Algorithm 2 Projected PG-DPO (P-PGDPO): Warm-up Training & Deployment

Stage 1: Warm-up Training
Require: Inputs of Algorithm 1; warm-up iterations K_0
Ensure: Stabilised parameters (θ^*, ϕ^*)

- 1: Run Algorithm 1 for K_0 iterations to obtain (θ^*, ϕ^*)

Stage 2: Deployment at state (t, X, \mathbf{Y})
Require: State (t, X, \mathbf{Y}) ; parameters (θ^*, ϕ^*) ; Monte-Carlo rollouts M_{MC} , steps N'
Ensure: Near-optimal controls $(\pi^{\text{PMP}}, C^{\text{PMP}})$

- 2: Initialise $\mathcal{L}, \mathcal{L}_x, \mathcal{L}_Y \leftarrow \emptyset$
 - 3: **for** $j = 1$ **to** M_{MC} **do**
 - 4: Simulate path from (t, X, \mathbf{Y}) with $(\pi_{\theta^*}, C_{\phi^*})$ using N' steps. Let $t'_0 = t$.
 - 5: Compute realized reward for path j :
 - 6:
$$J^{(j)} \leftarrow \sum_{n=0}^{N'-1} e^{-\delta(t_n - t'_0)} U(C_{t_n}^{(j)}) \Delta t' + \kappa e^{-\delta(T - t'_0)} U(X_T^{(j)})$$
 - 7: Evaluate $\lambda_t^{(j)}, \partial_x \lambda_t^{(j)}, \partial_{\mathbf{Y}} \lambda_t^{(j)}$ (costates at $t'_0 = t$) via BPTT on $J^{(j)}$ and append to lists $\mathcal{L}, \mathcal{L}_x, \mathcal{L}_Y$.
 - 8: **end for**
 - 9: Compute $\hat{\lambda}_t, \widehat{\partial_x \lambda}_t, \widehat{\partial_{\mathbf{Y}} \lambda}_t$ ▷ E.g., by averaging estimates from lists $\mathcal{L}, \mathcal{L}_x, \mathcal{L}_Y$
 - 10: $C^{\text{PMP}} \leftarrow (U')^{-1}(e^{\delta t} \hat{\lambda}_t)$ ▷ Using PMP FOC Eq. (8)
 - 11: Compute π^{PMP} via PMP FOC Eq. (15) ▷ Using estimated costates/derivatives
 - 12: **return** $(\pi^{\text{PMP}}, C^{\text{PMP}})$
-

parameters (θ^*, ϕ^*) obtained from Stage 1. For each simulated path $j = 1, \dots, M_{MC}$, calculate its realized reward $J^{(j)}(t_{\text{deploy}}, X_k, \mathbf{Y}_k; \theta^*, \phi^*)$ (using discounting relative to t_{deploy} as in Algorithm 2) and apply BPTT to obtain the costate estimates $\lambda_{\text{deploy}}^{(j)}, \partial_x \lambda_{\text{deploy}}^{(j)}, \partial_{\mathbf{Y}} \lambda_{\text{deploy}}^{(j)}$ specifically at the starting node t_{deploy} for that path j . The final “stabilized” estimates are then computed by averaging these values across the M_{MC} paths:

$$\lambda_{\text{deploy}} \approx \frac{1}{M_{MC}} \sum_{j=1}^{M_{MC}} \lambda_{\text{deploy}}^{(j)}, \quad \partial_x \lambda_{\text{deploy}} \approx \frac{1}{M_{MC}} \sum_{j=1}^{M_{MC}} \partial_x \lambda_{\text{deploy}}^{(j)}, \quad \partial_{\mathbf{Y}} \lambda_{\text{deploy}} \approx \frac{1}{M_{MC}} \sum_{j=1}^{M_{MC}} \partial_{\mathbf{Y}} \lambda_{\text{deploy}}^{(j)}$$

This averaging acts as a Monte Carlo estimation step, significantly reducing the variance inherent in the single-path BPTT estimates derived during Stage 1 and providing more robust inputs for the PMP formulas.

Next, we plug these **averaged costate estimates** $(\lambda_{\text{deploy}}, \partial_x \lambda_{\text{deploy}}, \partial_{\mathbf{Y}} \lambda_{\text{deploy}})$ directly into the analytical formulas derived from the Pontryagin Maximum Principle’s first-order conditions (Section 2.2). The optimal consumption at t_{deploy} is calculated as:

$$C_{\text{deploy}}^{\text{PMP}} = (U')^{-1}(e^{\delta t_{\text{deploy}}} \lambda_{\text{deploy}}).$$

The optimal investment portfolio at t_{deploy} is calculated as:

$$\begin{aligned} \pi_{\text{deploy}}^{\text{PMP}} = & -\frac{1}{X_k \partial_x \lambda_{\text{deploy}}} \Sigma^{-1}(t_{\text{deploy}}, \mathbf{Y}_k) \left\{ \lambda_{\text{deploy}} [\boldsymbol{\mu}(t_{\text{deploy}}, \mathbf{Y}_k) - r(t_{\text{deploy}}, \mathbf{Y}_k) \mathbf{1}] \right. \\ & \left. + (\boldsymbol{\sigma}(t_{\text{deploy}}, \mathbf{Y}_k) \boldsymbol{\rho} \boldsymbol{\sigma}_{\mathbf{Y}}(t_{\text{deploy}}, \mathbf{Y}_k)) (\partial_{\mathbf{Y}} \lambda_{\text{deploy}}) \right\}. \end{aligned} \quad (15)$$

(This formula aligns with Eq. (11), where λ_{deploy} corresponds to V_x , $\partial_x \lambda_{\text{deploy}}$ to V_{xx} , and $\partial_{\mathbf{Y}} \lambda_{\text{deploy}}$ to $V_{x\mathbf{Y}}$ at state $(t_{\text{deploy}}, X_k, \mathbf{Y}_k)$.)

Finally, these analytically computed values $(C_{deploy}^{\text{PMP}}, \boldsymbol{\pi}_{deploy}^{\text{PMP}})$, based on the averaged costate estimates, are used as the control actions for the state $(t_{deploy}, X_k, \mathbf{Y}_k)$ during deployment.

In summary, the Projected PG-DPO (P-PGDPO) approach performs a short warm-up training (Stage 1) using the baseline PG-DPO process to obtain a policy (θ^*, ϕ^*) whose BPTT generates reasonably stable costate estimates. It then leverages these estimates in Stage 2, refining them through Monte Carlo averaging at the point of deployment and plugging them into the known analytical structure of the optimal control derived from PMP. This strategy can significantly reduce the overall computational burden while yielding high-quality, near-optimal controls. The Monte Carlo averaging step in Stage 2 is crucial for obtaining reliable inputs for the PMP formulas from the potentially noisy single-path estimates.

3.3 Rationale for the Projected PG-DPO (P-PGDPO) Approach

In continuous-time financial models, where the dynamics of investor wealth X_t and exogenous state variables \mathbf{Y}_t are modeled by stochastic differential equations (SDEs), the Value Function $V(t, X_t, \mathbf{Y}_t)$ for a dynamic optimization problem typically solves a Hamilton–Jacobi–Bellman (HJB) partial differential equation (PDE) (e.g., Fleming and Soner, 2006; Yong and Zhou, 2012). This HJB equation exhibits a **parabolic** form. The specific nature of its parabolicity is primarily determined by the **diffusion coefficients** of the underlying SDEs, namely $\boldsymbol{\sigma}$ (related to assets) and $\boldsymbol{\sigma}_Y$ (related to state variables). While the first-order drift terms (involving $\boldsymbol{\mu}, \boldsymbol{\mu}_Y$) are crucial for the solution’s properties, they do not affect the parabolicity classification, which is mainly governed by the second-order diffusion terms.

The behavior of the diffusion matrix $a(t, x, \mathbf{y})$ (the matrix multiplying second-order derivatives in the HJB equation) allows for classifying parabolic PDEs into three main classes (see, e.g., Evans, 2022). This classification significantly impacts the **regularity** (smoothness) of the Value Function V and its associated Costates (the first-order derivatives ∇V) (cf. Evans, 2022, Ch. 6-7). Costates represent the sensitivity of the Value Function, and Pontryagin’s Maximum Principle links optimal Costates to the optimal policy. The core idea of Projected PG-DPO (P-PGDPO) involves estimating Costates and their derivatives via BPTT and using these estimates in the PMP formulas. Therefore, the regularity of the Costates—tied to the model’s parabolicity class—directly affects the difficulty of Costate estimation and the effectiveness of the P-PGDPO method.

Models falling into classes (U) and (H) are expected to possess sufficiently regular Costates, providing a favorable setting for the estimation required by the Projected PG-DPO (P-PGDPO) method. The numerical experiments in this paper are conducted using models belonging to classes (U) or (H), where P-PGDPO effectively leverages the expected regularity of the Costates. The method is particularly effective as it generally avoids visiting degenerate boundaries during practical implementation.

Building upon this expected regularity, a more formal mathematical justification for the P-PGDPO approach can be provided. The objective is to establish that if the policy (π, c) obtained from the Stage 1 warm-up phase satisfies a sufficiently small Pontryagin first-order condition (FOC) residual ε , then the feedback policy $\hat{\pi}$ constructed in Stage 2 using BPTT estimates $\hat{\lambda}$ (with BPTT estimation error δ_{BPTT}) will be close to the true optimal policy π^* . This analysis relies on certain standing assumptions concerning parabolic regularity and the FOC gap, which are formally stated as Assumption 6 and 7 in Appendix C. We use $L^{q,p}(Q_T)$ to denote the standard mixed space-time Lebesgue norm over the domain $Q_T = (0, T) \times \Omega \subseteq \mathbb{R}^{d+1}$, as detailed in Appendix C.

The main result of this analysis is encapsulated in the following theorem, the proof of which is detailed in Appendix C along with supporting lemmas and propositions.

Theorem 1 (Policy Gap Bound). *Under Assumptions 6 and 7 (detailed in Appendix C), let (π, c) be the policy from Stage 1 satisfying the FOC-gap condition $\|\mathcal{R}_{\text{FOC}}(\pi, c; \lambda)\|_{L^{q,p}} \leq \varepsilon$, where*

Table 1: Classification of Parabolic HJB PDEs in Financial Models

Class	Diffusion Matrix Property	$a(t, x, \mathbf{y})$	SDE Coefficient Requirements and Dynamic Portfolio Examples
<p>(U) Uniformly Elliptic</p> <p>(\implies Value Function / Costate very smooth)</p>	Uniformly positive definite across the state space		<p>The diffusion coefficients $\boldsymbol{\sigma}$ (for wealth X_t) and $\boldsymbol{\sigma}_Y$ (for state \mathbf{Y}_t) are such that the resulting diffusion matrix in the HJB is non-zero and bounded below by a positive constant everywhere (e.g., $\boldsymbol{\sigma}\Psi\boldsymbol{\sigma}^\top$ and $\text{diag}(\boldsymbol{\sigma}_Y)\Phi\text{diag}(\boldsymbol{\sigma}_Y)^\top$ uniformly positive definite). Drift coefficients $(\boldsymbol{\mu}, \boldsymbol{\mu}_Y)$ are also sufficiently regular (e.g., Lipschitz).</p> <p>Examples: Merton's portfolio problem with constant coefficients ($\mu, \sigma > 0, r$ are constants); models with state-dependent volatility that remains strictly positive; the multi-asset OU model in Section 2.3.1 (if asset volatilities $\sigma_i > 0$, factor volatility $\sigma_Y > 0$, and Ψ is positive definite).</p>
<p>(H) Hypo-elliptic</p> <p>(\implies Value Function / Costate smooth in relevant regions)</p>	May degenerate (even globally). Regularity is achieved if the system structure satisfies conditions like Hörmander's (i.e., Lie brackets of vector fields span the tangent space). The problem might be uniformly elliptic on compact subsets of interest.		<p>Diffusion coefficients ($\boldsymbol{\sigma}$ or $\boldsymbol{\sigma}_Y$) can become zero at certain points within the domain. However, interaction with non-zero drift terms or other diffusion terms maintains regularity.</p> <p>Examples: The multi-asset multi-factor model in Section 2.3.2 (if some factor volatilities in $\boldsymbol{\sigma}_Y$ can be zero at certain states but the overall system structure, possibly involving κ_Y, ensures hypo-ellipticity); a Vasicek interest rate model affecting asset returns μ but not σ.</p>
<p>(D) Degenerate at the Boundary</p> <p>(\implies Value Function / Costate regularity may break down near the boundary)</p>	Degenerates ($\rightarrow 0$) as the state approaches a boundary.		<p>The diffusion coefficients $\boldsymbol{\sigma}$ or $\boldsymbol{\sigma}_Y$ (or the combined diffusion matrix) approach zero as a state variable (e.g., wealth, volatility, interest rate) approaches a boundary (typically 0).</p> <p>Examples: CIR (Cox-Ingersoll-Ross) interest rate/volatility model (diffusion term like $\sigma_Y\sqrt{Y_t}$); Heston stochastic volatility model (asset diffusion term like $\sigma\sqrt{v_t}$).</p>

$\lambda = \nabla V^{\pi,c}$. Let π^* be the true optimal policy, and let $\hat{\pi} = F(\hat{\lambda})$ be the policy deployed in Stage 2 using BPTT estimates $\hat{\lambda}$, where F is the explicit mapping from costates $(\lambda, \nabla\lambda)$ to controls derived from the PMP FOCs. Assume F is locally Lipschitz continuous with constant C_F . If the BPTT estimation error $\|\hat{\lambda} - \nabla V^{\pi,c}\|_{L^{q,p}} \leq \delta_{\text{BPTT}}$ (where δ_{BPTT} quantifies the precision of BPTT-derived costate estimates relative to Stage 1 costates), then the policy gap is bounded by:

$$\boxed{\|\hat{\pi} - \pi^*\|_{L^{q,p}} \leq C_{\text{tot}}(\delta_{\text{BPTT}} + \varepsilon)}$$

Here, C_{tot} is a constant that depends on C_F and the constant C_v'' (derived from Proposition C.2 in Appendix C).

The proof of Theorem 1 follows a logical chain: the FOC-gap ($\leq \varepsilon$) implies that errors in PDE coefficients and source terms are of order $O(\varepsilon)$. These, in turn, through PDE stability, imply that the error in the value function’s gradient $E_v = \|\nabla V^{\pi,c} - \nabla V^*\|_{L^{q,p}}$ is also of order $O(\varepsilon)$. Combining this with the BPTT estimation error δ_{BPTT} leads to the final policy-gap bound. The detailed arguments, including the necessary lemmas and propositions, are provided as sketches in Appendix C. It is important to note that all constants involved depend quantitatively on model parameters, PDE regularity, and utility specifications. Full rigorous proofs would require meticulous tracking of these dependencies and bounds.

Our formal analysis (detailed in Appendix C) demonstrates that under suitable regularity conditions, particularly uniform parabolicity, a small Pontryagin first-order condition (FOC) gap (ε) achieved during the Stage 1 warm-up guarantees that the BPTT-derived costate estimates are $O(\varepsilon)$ -close to the true optimal costates (up to the BPTT estimation error δ_{BPTT}). This provides a rigorous justification for the core idea of the P-PGDPO method: substituting these rapidly stabilizing and sufficiently accurate costate estimates into the analytical PMP formulas yields a near-optimal policy $\hat{\pi}$ with an error bound of $O(\varepsilon + \delta_{\text{BPTT}})$ (Theorem 1).

However, extending this rigorous proof framework to settings beyond uniform parabolicity, such as hypo-elliptic (*H-class*, (Hörmander, 1967)) or boundary-degenerate (*D-class*, (Oleinik, 2012)) models, or to general non-affine systems, faces significant analytical challenges, as key assumptions (like global L^p regularity or the costate floor) may no longer hold.

Despite these formal hurdles, the fundamental *algorithmic rationale* underpinning the P-PGDPO approach remains persuasive for broader applicability. Neither Pontryagin’s Maximum Principle (PMP) (Pontryagin, 2014; Yong and Zhou, 2012) nor backpropagation-through-time (BPTT) (Goodfellow, 2016) are inherently limited to uniformly parabolic or affine settings. The P-PGDPO strategy leverages the potentially advantageous decoupling of the problem into: (i) estimating potentially simpler or faster-converging costate functions via BPTT, and (ii) utilizing the robust analytical structure of PMP to construct the control.

This rationale, strongly supported by the numerical success demonstrated even in high dimensions for the affine benchmark case (Section 4), suggests that PG-DPO (especially the P-PGDPO variant) holds promise as a practical tool for a wider class of challenging continuous-time control problems. Nonetheless, confirming its effectiveness and potentially refining the theoretical guarantees for models outside the strictly regular class analyzed here remains an important avenue for future research, likely requiring tailored analysis or different analytical techniques (e.g., focusing on regions predominantly visited by the state process).

4 Numerical Experiments

In this section, we conduct numerical experiments to evaluate the performance and scalability of the proposed PG-DPO framework (both Baseline and Projected PG-DPO (P-PGDPO) variants). We focus on the multi-asset, multi-factor Ornstein-Uhlenbeck (OU) portfolio optimization problem introduced in Section 2.3.2. The objective is to maximize the expected utility of terminal wealth, $J = \mathbb{E}[U(X_T)]$, using a CRRA utility function with risk aversion $\gamma = 2.0$.

For these experiments, we specialize the general model by assuming no intermediate consumption (i.e., $C_t \equiv 0$) and focus solely on the utility from terminal wealth (effectively setting the bequest weight $\kappa = 1$ if $U(X_T)$ is the direct objective, or adjusting κ appropriately if a specific HARA utility form with $a \neq 0$ was being precisely mapped).

This specific affine model setting allows for comparison against a semi-analytical benchmark solution derived from the HJB equation (details in Appendix B.2). Furthermore, to provide a comprehensive assessment against other contemporary deep learning techniques for high-dimensional control problems, we also compare our PG-DPO framework with the Deep BSDE method (Han et al., 2018; Weinan, 2017). The Deep BSDE approach reformulates the stochastic control problem in terms of a system of backward stochastic differential equations, approximating the unknown components of the solution (typically related to the value function gradient or control variables) using neural networks. These networks are trained by minimizing the error incurred in satisfying the BSDE dynamics and terminal conditions through Monte Carlo simulation.

We compare the policies generated by Baseline PG-DPO, Projected PG-DPO (P-PGDPO), and the Deep BSDE method against the HJB-based benchmark using the Root Mean Squared Error (RMSE) metric across various dimensions, scaling up to $n=50$ assets and $k=10$ state factors. For complete details on the specific parameter values, the implementations of PG-DPO and Deep BSDE (including network architectures and training setups), benchmark computation, and evaluation procedures, please refer to Appendix D. The subsequent subsections present and analyze the results of these comparative experiments.

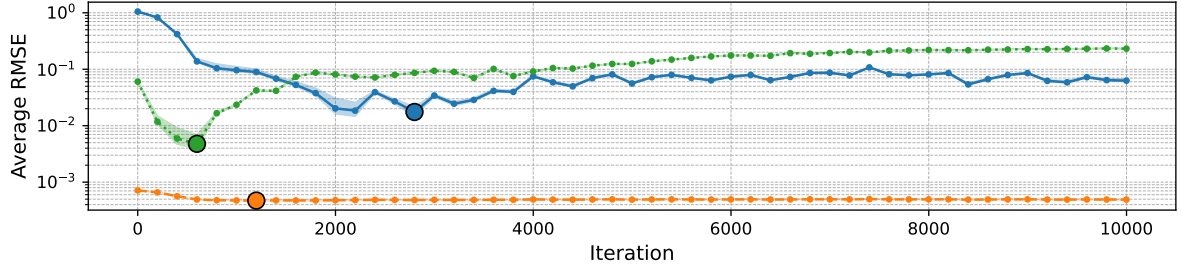
4.1 Convergence Speed and Accuracy Analysis

This section quantitatively compares the convergence speed and final accuracy of the proposed PG-DPO framework (Baseline and Projected PG-DPO (P-PGDPO) variants) against the Deep BSDE method. We analyze their performance across various dimensional settings, focusing on how the number of assets (n) and the number of state factors (k) impact accuracy. Figure 1 (Note: Assuming you will update the figure label in your main document if it includes Deep BSDE results) displays the average Root Mean Squared Error (RMSE) between the learned/derived policies and the benchmark optimal policy. The RMSE is plotted against training epochs on a logarithmic scale for configurations with $k = 10$ state variables and varying numbers of assets ($n = 1, 10, 50$).

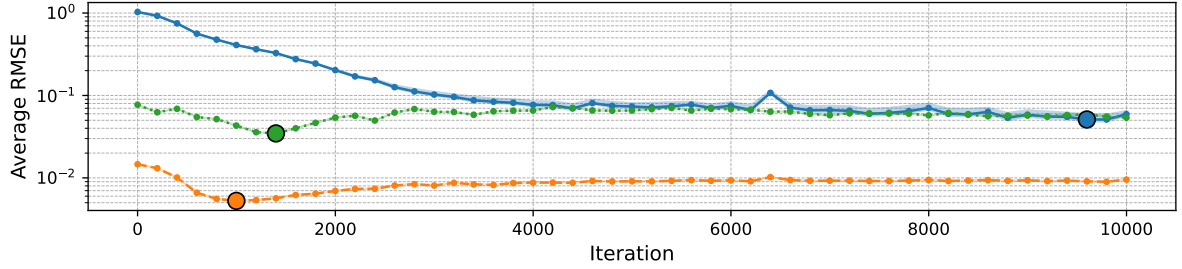
The RMSE for P-PGDPO represents the error of the total portfolio policy π^{PMP} (Eq. (11)), which combines myopic and hedging components. As detailed in Section 4.2, the myopic component’s error is typically negligible ($O(10^{-7})$). Thus, the total RMSE for P-PGDPO is almost entirely driven by the accuracy of estimating the *hedging component* using BPTT-derived costate derivatives, $\partial_{\mathbf{Y}} \lambda_t^*$.

Table 2 summarizes the minimum achieved policy RMSE and the epochs at which these minima were observed for the $k = 10$ scenario with varying n . A consistent observation is the superior performance of the P-PGDPO method, which achieves significantly lower RMSE values compared to both Baseline PG-DPO and Deep BSDE across all tested asset dimensions. For instance, with $n = 1, k = 10$, P-PGDPO’s minimum RMSE is approximately an order of magnitude better than Deep BSDE and two orders of magnitude better than Baseline PG-DPO. Deep BSDE generally performs between the Baseline and P-PGDPO methods. While P-PGDPO maintains its lead as n increases to 50, the performance gap between P-PGDPO and Deep BSDE tends to narrow, suggesting that the increasing dimensionality of n poses challenges even for the PMP-based analytical solution, possibly due to the ill-conditioning of the covariance matrix Σ . All methods show an increase in RMSE as n grows, indicating the inherent difficulty of high-dimensional asset allocation.

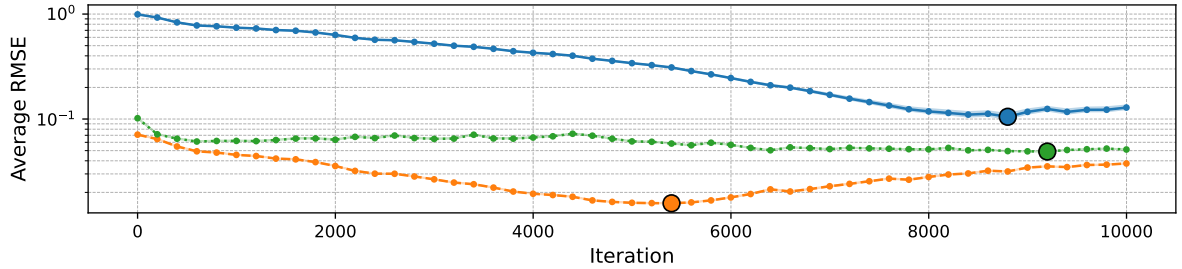
To further investigate the distinct effects of asset dimensionality (n) versus factor dimensionality (k), we conducted two additional sets of experiments.



(a) $n = 1, k = 10$



(b) $n = 10, k = 10$



(c) $n = 50, k = 10$

Figure 1: Average policy RMSE comparison between Baseline PG-DPO (e.g., blue), Projected PG-DPO (P-PGDPO) (e.g., orange), and Deep BSDE (e.g., green) relative to the benchmark solution across different asset dimensions (n) with $k = 10$ factors fixed. Values averaged over k evaluation ‘slices.’ For each slice $j = 1, \dots, k$, the evaluation (e.g., for RMSE calculation or visualization) focuses on state factor Y_j , while other factors $Y_l, l \neq j$, are held constant at their respective long-term means θ_{Y_l} . Further details on the evaluation methodology are provided in Appendix D. Note the logarithmic scale on the y -axis.

First, Table 3 presents results where the number of assets is fixed at $n = 1$, and the number of state factors k is varied ($k = 1, 5, 10$). In this scenario, the performance of all three methodologies remains relatively stable across different values of k . For P-PGDPO, the RMSE even shows a slight improvement as k increases, possibly due to more information being available for costate estimation. Deep BSDE and Baseline PG-DPO also exhibit no significant degradation in performance. This suggests that, for a small number of assets, the ‘curse of dimensionality’ associated with an increasing number of state factors (k) is largely managed by these neural network-based approaches. The underlying PMP structure or BSDE formulation appears robust to the increase in k when n is small and fixed, with Monte Carlo sampling and function approximation being the primary challenges rather than ill-conditioned linear algebra.

Second, Table 4 shows results where the number of state factors is fixed at $k = 2$, and the

Table 2: Summary of Minimum Policy RMSE and Convergence Epochs

Dimension (n assets, $k = 10$ factors)	Method	Min. Policy RMSE	Epochs at Min.
n=1, k=10	Baseline PG-DPO	1.75×10^{-2}	2800
	P-PGDPO	4.72×10^{-4}	1200
	Deep BSDE	4.78×10^{-3}	600
n=10, k=10	Baseline PG-DPO	5.11×10^{-2}	9600
	P-PGDPO	5.26×10^{-3}	1000
	Deep BSDE	3.46×10^{-2}	1400
n=50, k=10	Baseline PG-DPO	1.05×10^{-1}	8800
	P-PGDPO	1.58×10^{-2}	5400
	Deep BSDE	4.90×10^{-2}	9200

Note: Minimum Policy RMSE values are averaged across k evaluation 'slices.' For each slice $j = 1, \dots, k$, the evaluation (e.g., for RMSE calculation) focuses on state factor Y_j , while other factors $Y_l, l \neq j$, are held constant at their respective long-term means $\theta_{Y,l}$. Further details on the evaluation methodology are provided in Appendix D. Epochs indicate the recorded iteration number when the minimum average RMSE was observed; evaluations and logging were performed every 200 iterations.

Table 3: Summary of Minimum Policy RMSE and Convergence Epochs for $n = 1$ (Varying k)

k factors ($n = 1$ asset)	Method	Min. Policy RMSE	Epochs at Min.
1	Baseline PG-DPO	3.26×10^{-2}	1000
	P-PGDPO	1.20×10^{-3}	800
	Deep BSDE	7.39×10^{-3}	800
5	Baseline PG-DPO	3.71×10^{-2}	1400
	P-PGDPO	2.64×10^{-4}	800
	Deep BSDE	1.02×10^{-2}	1400
10	Baseline PG-DPO	1.75×10^{-2}	2800
	P-PGDPO	4.72×10^{-4}	1200
	Deep BSDE	4.78×10^{-3}	600

Table 4: Summary of Minimum Policy RMSE and Convergence Epochs for $k = 2$ (Varying n)

n assets ($k = 2$ factors)	Method	Min. Policy RMSE	Epochs at Min.
1	Baseline PG-DPO	4.77×10^{-2}	1200
	P-PGDPO	1.98×10^{-4}	800
	Deep BSDE	4.63×10^{-3}	3400
10	Baseline PG-DPO	1.12×10^{-1}	4000
	P-PGDPO	1.22×10^{-2}	1400
	Deep BSDE	2.32×10^{-2}	2600
50	Baseline PG-DPO	2.24×10^{-1}	7200
	P-PGDPO	5.55×10^{-2}	4400
	Deep BSDE	1.88×10^{-1}	4400

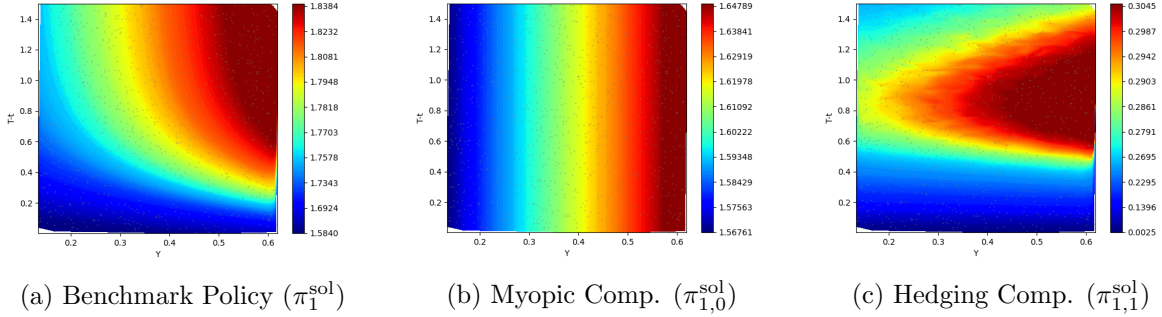


Figure 2: Benchmark (analytical) solution components for the first asset ($i = 1$) in the $n = 50, k = 10$ case, plotted against Y_1 at a representative time-to-maturity $T-t$ (e.g., $t = (T-T_0)/2$ if T_0 is initial time, assuming $T = 1.5$ is the horizon from $t = 0$; thus, for instance, at $t = 0.75$ or time-to-maturity 0.75). Other state factors $Y_{j \neq 1}$ are held at their long-term means $\theta_{Y,j}$. From left to right: total optimal policy, its myopic component, and its intertemporal hedging component. These serve as the ground truth.

number of assets n is varied ($n = 1, 10, 50$). In stark contrast to the previous case, increasing n leads to a significant deterioration in performance for all three methods. Baseline PG-DPO shows the most substantial increase in RMSE. While P-PGDPO still yields the lowest RMSE, its error also increases considerably with n . Deep BSDE’s performance also degrades, approaching that of Baseline PG-DPO for $n = 50$. This pronounced degradation with increasing n (even for a small k) points towards a different kind of challenge not solely related to the dimensionality of the state space for function approximation. A primary suspect is the numerical instability arising from the asset covariance matrix Σ . As n increases, Σ ($n \times n$) is more likely to become ill-conditioned (i.e., have a high condition number). The optimal policy calculation, particularly in the PMP framework (Eq. (11)), involves the inverse Σ^{-1} . If Σ is ill-conditioned, any small errors in the estimated costates or market parameters can be greatly amplified by Σ^{-1} , leading to large errors in the computed policy. This suggests that the “curse” associated with large n is not just about learning a higher-dimensional policy function but also about the increasing fragility of the underlying mathematical problem structure due to the properties of Σ . The problem itself becomes “damaged” or numerically challenging, impacting any method that relies on or implicitly reflects this structure.

These findings underscore that while neural network approaches have made significant strides in handling high-dimensional state spaces (related to k), the challenges posed by a large number of decision variables (assets n), especially when intertwined with ill-conditioned covariance matrices, require further attention. Strategies such as covariance matrix shrinkage or other regularization techniques applied prior to or within the optimization might be necessary to effectively address this “asset-dimension curse”.

4.2 High-Dimensional Performance Analysis ($n = 50, k = 10$)

We now visually examine the performance of the three methodologies in the most challenging setting considered: $n = 50$ assets and $k = 10$ state factors. This high-dimensional scenario, where traditional DP methods are intractable, serves to highlight the distinct capabilities and limitations of each approach. As a reference, Figure 2 displays the benchmark analytical solution for the first asset (π_1^{sol}), decomposed into its myopic ($\pi_{1,0}^{\text{sol}}$) and intertemporal hedging ($\pi_{1,1}^{\text{sol}}$) components. The hedging component is clearly non-trivial and exhibits complex dependencies on both the state variable Y_1 and time-to-maturity, underscoring its importance for optimal allocation.

Figure 3 provides a side-by-side comparison of the policies learned by Baseline PG-DPO,

Projected PG-DPO (P-PGDPO), and Deep BSDE, alongside their respective errors, for the first asset. These plots correspond to iterations where each method achieved its (near) optimal performance in the $n = 50, k = 10$ setting, as indicated in Table 2 (e.g., iteration 5400 for P-PGDPO, which is the nearest logged checkpoint to the observed minimum RMSE at iteration 5399, as evaluations were performed every 200 iterations).

The Baseline PG-DPO method (Figure 3a,b), despite utilizing a standard neural network architecture (detailed in Appendix D.2), struggles significantly. While its learned policy exhibits some non-linear structure, it bears little resemblance to the benchmark, and the corresponding error is extremely large. This performance visually confirms the poor quantitative results in Table 2 and highlights the difficulty of directly approximating the high-dimensional optimal policy function using a neural network without leveraging more structural information from the problem.

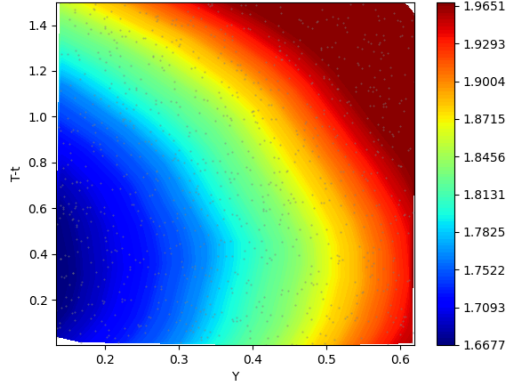
The Deep BSDE method (Figure 3e,f) shows a marked improvement over the Baseline. Its learned policy qualitatively resembles the myopic component of the benchmark (cf. Figure 2b), primarily capturing dependencies on the state variable Y_1 . However, the policy largely fails to capture the complex intertemporal hedging demands. The error plot for Deep BSDE (Figure 3f) shows significant discrepancies in regions where hedging is important, suggesting that the hedging component is largely absent from the Deep BSDE solution. This difficulty in capturing hedging demands can be attributed to several factors. The Deep BSDE method primarily focuses on matching the terminal condition and ensuring consistency of the value process Y_t and the gradient-related process Z_t (approximating first-order derivatives of the value function) through its loss function. Intertemporal hedging, however, critically depends on the mixed second-order derivative V_{xy} , which is not explicitly represented or directly targeted by the standard two-network Deep BSDE architecture. Furthermore, the loss function penalizes inaccuracies in Z_t primarily through a quadratic martingale term. Consequently, small errors in estimating the gradient components relevant to V_{xy} might have a limited impact on the overall training objective but can be significantly magnified when constructing the policy, especially after multiplication by the potentially ill-conditioned inverse covariance matrix Σ^{-1} in high-dimensional settings. As a result, while the Deep BSDE approach can effectively learn the dominant myopic component of the policy, it may struggle to precisely fit the more nuanced intertemporal hedging patterns.

In stark contrast, the Projected PG-DPO (P-PGDPO) method (Figure 3c,d) delivers a policy that is visually almost identical to the benchmark total policy (Figure 2a). The corresponding error is substantially smaller than that of the other two methods. This superior performance underscores the efficacy of its decoupled learning structure: first estimating costates via BPTT and stabilizing them through Monte Carlo averaging, then analytically constructing the policy using the PMP FOCs.

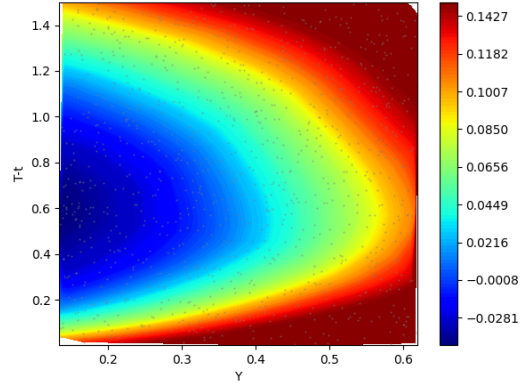
The remarkable accuracy of P-PGDPO is further elucidated by decomposing its policy into myopic and hedging components, as shown in Figure 4 (results from iteration 5400). The myopic component (Figure 4a) is virtually identical to the benchmark myopic component, with its error (Figure 4c) being negligible ($O(10^{-7})$). The hedging component derived by P-PGDPO (Figure 4b) also successfully captures the complex shape of the benchmark hedging demand (Figure 2c). The remaining error in the hedging component (Figure 4d) dictates the overall error of the P-PGDPO policy. This residual hedging error is likely not due to a fundamental flaw in the P-PGDPO algorithm itself but rather a consequence of the numerical challenges inherent in high-dimensional asset allocation. Specifically, the hedging term in the PMP FOC involves Σ^{-1} :

$$\pi^{\text{hedge}} = -\frac{1}{X_t V_{xx}} \underbrace{\Sigma^{-1}}_{\text{cond num can be large for } n \uparrow} (\sigma \rho \sigma_Y) V_{xY}.$$

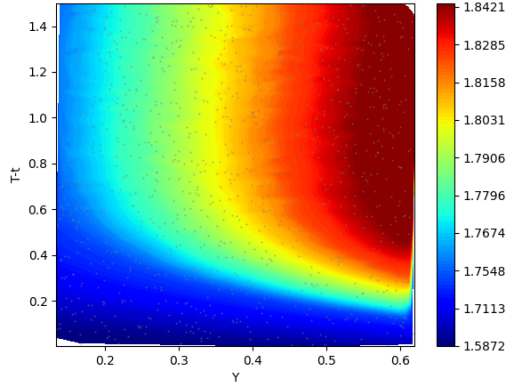
For $n = 50$, the 50×50 covariance matrix Σ can easily become ill-conditioned. Even if the BPTT-derived estimate for V_{xY} is quite accurate, any small residual noise can be significantly



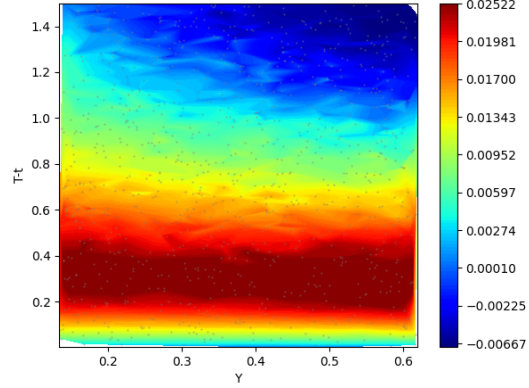
(a) Baseline Policy ($\pi_{1,\theta}$)



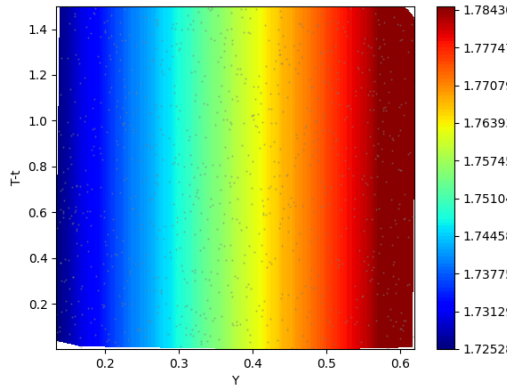
(b) Baseline Error



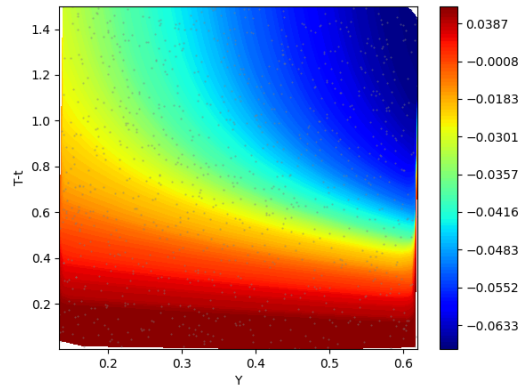
(c) P-PGDPO Policy (π_1^{PMP})



(d) P-PGDPO Error



(e) Deep BSDE Policy (π_1^{BSDE})



(f) Deep BSDE Error

Figure 3: Comparison of total policies (left column) and policy errors (right column) for the first asset ($i = 1$) across Baseline PG-DPO (top row), Projected PG-DPO (P-PGDPO) (middle row), and Deep BSDE (bottom row) in the $n = 50, k = 10$ case. Results shown at (near) optimal iterations for each method (e.g., iteration 5400 for P-PGDPO), plotted against Y_1 at a representative time-to-maturity $T - t$ (consistent with Figure 2). Other state factors $Y_{j \neq 1}$ are held at their long-term means $\theta_{Y,j}$. Errors use a symmetric logarithmic (symlog) scale. Different color bar ranges reflect varying policy/error magnitudes.

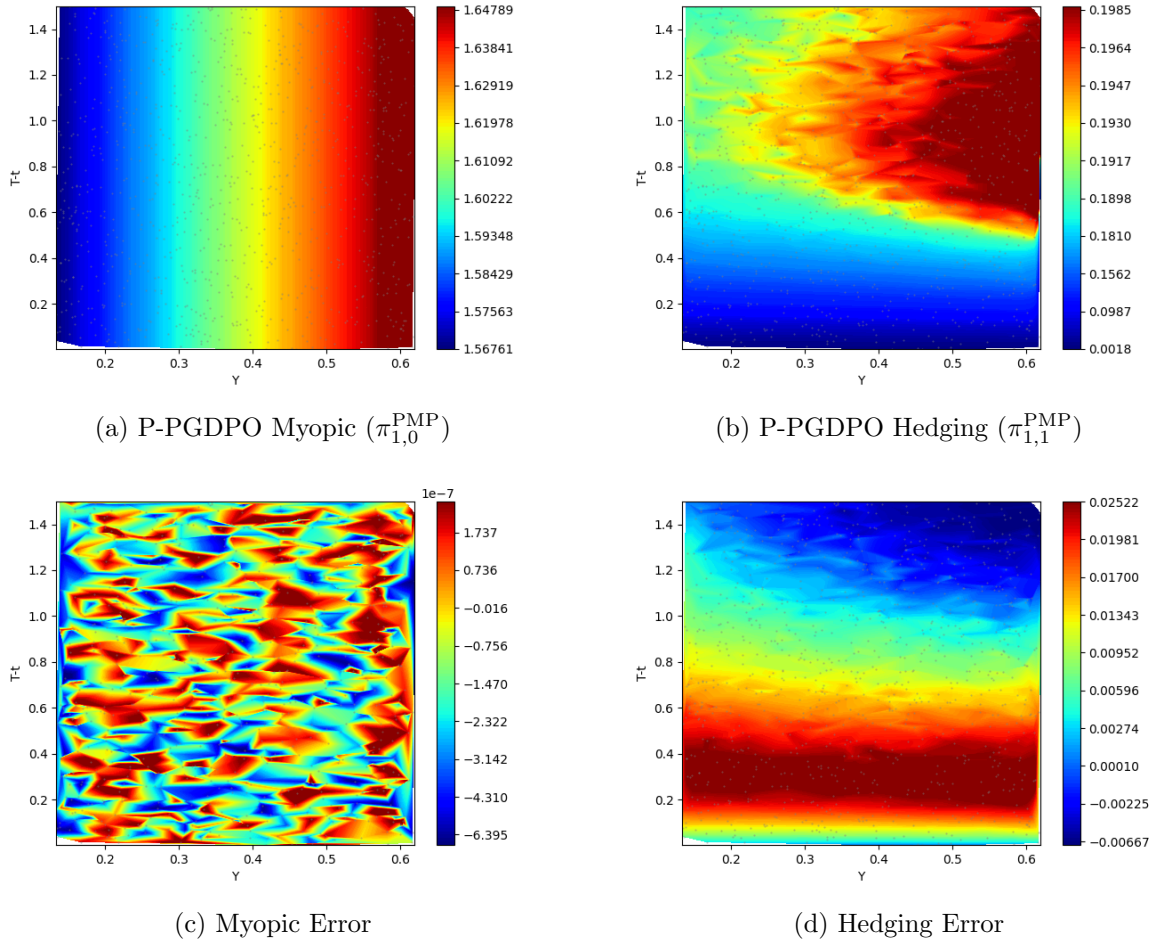


Figure 4: Decomposition of the Projected PG-DPO (P-PGDPO) policy for the first asset ($i = 1$) in the $n = 50, k = 10$ case (results from iteration 5400), plotted against Y_1 at a representative time-to-maturity $T - t$ (consistent with Figure 2). Other state factors $Y_{j \neq 1}$ are held at their long-term means $\theta_{Y,j}$. Top row: myopic and hedging components. Bottom row: their respective errors (symmetric logarithmic (symlog) scale). Note different color bar ranges.

amplified when multiplied by Σ^{-1} if its condition number is large. This amplification effect is the primary suspect for the observed hedging error.

In conclusion, the $n = 50, k = 10$ visualizations powerfully demonstrate that Projected PG-DPO (P-PGDPO) can effectively “break the dimensional barrier” where Baseline PG-DPO fails and Deep BSDE offers only a partial (myopic-focused) solution. The remaining inaccuracies in the hedging component point towards the need for addressing the ill-conditioning of the covariance matrix in very high asset dimensions.

5 Conclusion

This paper confronted the enduring “curse of dimensionality” in continuous-time portfolio optimization, a challenge that manifests distinctly with increasing asset numbers (n) versus state factors (k). Our numerical investigations (Section 4) revealed that while deep learning methods manage larger k relatively well, escalating n poses severe difficulties, particularly due to the ill-conditioning of asset covariance matrices. Furthermore, we identified that prevalent approaches like Deep BSDE, while proficient at capturing myopic policy components, often fail to ade-

quately represent crucial intertemporal hedging demands, a limitation rooted in their network architecture and loss functions which do not explicitly target the necessary second-order mixed derivatives of the value function (e.g., V_{xy}).

To surmount these obstacles, we introduced the *Pontryagin-Guided Direct Policy Optimization (PG-DPO)* framework, with its highly effective *Projected PG-DPO (P-PGDPO)* variant (Section 3.2). P-PGDPO distinctively leverages Pontryagin’s Maximum Principle (PMP) by first employing backpropagation-through-time (BPTT) to achieve rapidly stabilizing estimates of the Pontryagin costates and their derivatives (e.g., $\lambda_t, \partial_x \lambda_t, \partial_{\mathbf{Y}} \lambda_t$). These estimates are then analytically projected onto the manifold of PMP-optimal controls via the first-order conditions. This decoupling strategy proved remarkably successful, enabling P-PGDPO to tackle problems of previously prohibitive scales. For instance, in a challenging $n = 50$ asset, $k = 10$ factor environment, P-PGDPO achieved a total policy RMSE of 1.58×10^{-2} relative to the analytical benchmark, with the myopic component error being negligible ($O(10^{-7})$) and, critically, accurately reconstructing complex hedging terms (Section 4.2, Figure 4). The theoretical underpinnings of P-PGDPO are strengthened by our Policy Gap Bound (Theorem 1), which guarantees near-optimal policies given accurate costate estimation and a small FOC gap.

Despite its successes, P-PGDPO’s accuracy in representing hedging terms can be affected by the amplification of estimation noise through the inverse covariance matrix Σ^{-1} when n is large and Σ is ill-conditioned (Section 4.2). Concurrently, our experiments confirmed that Deep BSDE, while adept at matching myopic demands, struggles with learning the nuanced cross-derivative information essential for hedging, largely due to its architectural and objective function design (Figure 3). These observations highlight the distinct strengths and weaknesses of different deep learning paradigms in high-dimensional control.

The practical implications of P-PGDPO are significant. Its demonstrated ability to recover complex, non-linear hedging strategies in high dimensions suggests its potential applicability to large institutional portfolios, such as those involving numerous ETFs or derivative hedging. Moreover, the core principle of P-PGDPO—“estimate costates first, then derive policy”—holds promise for a broader class of problems, where PMP provides the necessary optimality structure (Section 3.3).

Future research will pursue several promising directions:

- Developing “P-PGDPO 2.0” by integrating Σ regularization or shrinkage techniques to mitigate the impact of ill-conditioned covariance matrices on hedging term estimation.
- Extending the P-PGDPO framework to incorporate portfolio constraints (e.g., no short-selling, leverage limits) and market frictions like transaction costs, by adapting the PMP conditions accordingly.
- Investigating the performance of P-PGDPO with non-HARA utility functions and behavioral finance objectives, and fully integrating the optimization of intermediate consumption policies (C_t).
- Validating the framework through rigorous backtesting on historical and simulated market data for non-affine models.
- Rigorously characterizing the precise range of financial models that satisfy the sufficient regularity assumptions for the P-PGDPO framework’s effectiveness.

In essence, PG-DPO, particularly its projected variant, demonstrates that the synergy between deep learning and the structural guidance of Pontryagin’s Maximum Principle can redefine the boundaries of solvability for high-dimensional continuous-time financial control problems.

Acknowledgments

This work was supported by the National Research Foundation of Korea (NRF) grant funded by the Korea government (MSIT) (RS-2025-00562904).

References

- Balduzzi, P. and Lynch, A. W. (1999). Transaction costs and predictability: Some utility cost calculations. *Journal of Financial Economics*, 52(1):47–78. 1
- Bellman, R. (1966). Dynamic programming. *science*, 153(3731):34–37. 1
- Bertsekas, D. P. and Tsitsiklis, J. N. (1995). Neuro-dynamic programming: an overview. In *Proceedings of 1995 34th IEEE conference on decision and control*, volume 1, pages 560–564. IEEE. 1
- Borkar, V. S. and Borkar, V. S. (2008). *Stochastic approximation: a dynamical systems viewpoint*, volume 9. Springer. 1
- Brandt, M. W., Goyal, A., Santa-Clara, P., and Stroud, J. R. (2005). A simulation approach to dynamic portfolio choice with an application to learning about return predictability. *The Review of Financial Studies*, 18(3):831–873. 1
- Campbell, J. Y., Chan, Y. L., and Viceira, L. M. (2003). A multivariate model of strategic asset allocation. *Journal of financial economics*, 67(1):41–80. 1
- Campbell, J. Y. and Viceira, L. M. (1999). Consumption and portfolio decisions when expected returns are time varying. *The Quarterly Journal of Economics*, 114(2):433–495. 1
- Davey, A. and Zheng, H. (2022). Deep learning for constrained utility maximisation. *Methodology and Computing in Applied Probability*, 24(2):661–692. 1
- Dong, H. and Kim, D. (2009). Parabolic and elliptic systems with vmo coefficients. C
- Duarte, V., Duarte, D., and Silva, D. H. (2024). Machine learning for continuous-time finance. *The Review of Financial Studies*, 37(11):3217–3271. 1
- Evans, L. C. (2022). *Partial differential equations*, volume 19. American Mathematical Society. 3.3
- Fleming, W. H. and Soner, H. M. (2006). *Controlled Markov processes and viscosity solutions*, volume 25. Springer Science & Business Media. 1, 3.3
- Garlappi, L. and Skoulakis, G. (2010). Solving consumption and portfolio choice problems: The state variable decomposition method. *The Review of Financial Studies*, 23(9):3346–3400. 1
- Goodfellow, I. (2016). Deep learning. 3.3
- Han, J., Jentzen, A., and E, W. (2018). Solving high-dimensional partial differential equations using deep learning. *Proceedings of the National Academy of Sciences*, 115(34):8505–8510. 1, 4, D.4
- Hörmander, L. (1967). Hypoelliptic second order differential equations. *Acta Mathematica*, 119:147–171. 3.3
- Huh, J. (2024). A pontryagin-guided neural policy optimization framework for merton’s portfolio problem. *arXiv preprint arXiv:2412.13101*. 3.1

- Karatzas, I., Lehoczky, J. P., and Shreve, S. E. (1987). Optimal portfolio and consumption decisions for a "small investor" on a finite horizon. *SIAM journal on control and optimization*, 25(6):1557–1586. 1
- Kim, T. S. and Omberg, E. (1996). Dynamic nonmyopic portfolio behavior. *The Review of Financial Studies*, 9(1):141–161. 2, 2.3.1, B.1
- Kopeliovich, Y. and Pokojovy, M. (2024). Portfolio optimization with feedback strategies based on artificial neural networks. *Finance Research Letters*, 69:106185. 1
- Kushner, H. J. and Yin, G. G. (2003). *Stochastic Approximation and Recursive Algorithms and Applications*. Springer Science & Business Media, New York. 1
- Liu, J. (2007). Portfolio selection in stochastic environments. *The Review of Financial Studies*, 20(1):1–39. 2
- Lynch, A. W. (2001). Portfolio choice and equity characteristics: Characterizing the hedging demands induced by return predictability. *Journal of Financial Economics*, 62(1):67–130. 1
- Merton, R. C. (1973). An intertemporal capital asset pricing model. *Econometrica: Journal of the Econometric Society*, pages 867–887. 1, 2
- Nguwi, J. Y., Penent, G., and Privault, N. (2024). A deep branching solver for fully nonlinear partial differential equations. *Journal of Computational Physics*, 499:112712. 1
- Oksendal, B. (2013). *Stochastic differential equations: an introduction with applications*. Springer Science & Business Media. 2.1, 2.1
- Oleinik, O. (2012). *Second-order equations with nonnegative characteristic form*. Springer Science & Business Media. 3.3
- Pennacchi, G. G. (2008). *Theory of asset pricing*. Pearson/Addison-Wesley Boston. 2.1
- Pontryagin, L. S. (2014). *Ordinary Differential Equations: Adiwes International Series in Mathematics*. Elsevier. 1, 2, 3.3
- Raissi, M., Perdikaris, P., and Karniadakis, G. E. (2019). Physics-informed neural networks: A deep learning framework for solving forward and inverse problems involving nonlinear partial differential equations. *Journal of Computational physics*, 378:686–707. 1
- Weinan, E. (2017). A proposal on machine learning via dynamical systems. *Communications in Mathematics and Statistics*, 1(5):1–11. 4, D.4
- Yong, J. and Zhou, X. Y. (2012). *Stochastic controls: Hamiltonian systems and HJB equations*, volume 43. Springer Science & Business Media. 1, 2, 2.2, (a), 3.3, 3.3
- Zhang, W. and Zhou, C. (2019). Deep learning algorithm to solve portfolio management with proportional transaction cost. In *2019 IEEE Conference on Computational Intelligence for Financial Engineering & Economics (CIFER)*, pages 1–10. IEEE. 1

A Derivation of the Adjoint Diffusion Coefficient via Itô’s Lemma

In the Pontryagin framework, the adjoint (or costate) process associated with the investor’s wealth X_t is identified with the partial derivative of the value function V . Concretely, we set $\lambda_t = V_X(t, X_t, \mathbf{Y}_t)$, where $\mathbf{Y}_t \in \mathbb{R}^k$ represents additional state variables and X_t is the investor’s scalar wealth process. Our goal in this section is to derive the diffusion coefficient corresponding

to the $d\mathbf{W}_t^X$ term in the backward SDE for λ_t , namely $\mathbf{Z}_t^{\lambda X}$ from BSDE (6), which plays a crucial role in determining the optimal portfolio via FOC (10).

Recall that under an optimal control $(\boldsymbol{\pi}_t^*, C_t^*)$, the wealth X_t^* evolves according to Eq. (4) and Eq. (5), and the k -dimensional state process \mathbf{Y}_t^* follows its own SDE, also presented in Section 2.2. The dynamics are driven by correlated Brownian motions $\mathbf{W}_t^X \in \mathbb{R}^n$ and $\mathbf{W}_t^Y \in \mathbb{R}^k$ with the joint covariance structure $\text{Cov}(d\mathbf{W}_t) = \begin{pmatrix} \Psi & \rho \\ \rho^\top & \Phi \end{pmatrix} dt$.

Since $\lambda_t = V_X(t, X_t, \mathbf{Y}_t)$, we apply Ito's multidimensional lemma to V_X . The differential $d\lambda_t$ can be expressed as:

$$\begin{aligned} d\lambda_t &= V_{Xt} dt + V_{XX} dX_t + V_{X\mathbf{Y}} d\mathbf{Y}_t \\ &\quad + \frac{1}{2} V_{XXX} (dX_t)^2 + V_{XX\mathbf{Y}} (dX_t) (d\mathbf{Y}_t)^\top + \frac{1}{2} \text{Tr}(V_{X\mathbf{Y}\mathbf{Y}} (d\mathbf{Y}_t)(d\mathbf{Y}_t)^\top), \end{aligned} \quad (16)$$

where subscripts denote partial derivatives (e.g., $V_{X\mathbf{Y}}$ is the gradient w.r.t \mathbf{Y} of V_X , $V_{X\mathbf{Y}\mathbf{Y}}$ is the Hessian w.r.t \mathbf{Y} of V_X).

Our objective is to identify the coefficient of $d\mathbf{W}_t^X$ in the expansion of $d\lambda_t$. This coefficient is precisely the process $\mathbf{Z}_t^{\lambda X}$ appearing in the BSDE (6). Substituting the SDEs for dX_t and $d\mathbf{Y}_t$ (from Section 2.2) into the Ito formula (16), we observe that terms involving $d\mathbf{W}_t^X$ arise directly from the diffusion part of the $V_{XX} dX_t$ term, and indirectly from the $V_{X\mathbf{Y}} d\mathbf{Y}_t$ term due to the correlation ρ between $d\mathbf{W}_t^X$ and $d\mathbf{W}_t^Y$. A careful application of Ito's lemma, considering the quadratic variation and covariation terms related to the covariance matrix $\begin{pmatrix} \Psi & \rho \\ \rho^\top & \Phi \end{pmatrix}$, allows isolation of the full coefficient multiplying $d\mathbf{W}_t^X$. Representing $\mathbf{Z}_t^{\lambda X}$ as a $1 \times n$ row vector, this process is found to be:

$$\mathbf{Z}_t^{\lambda X} = \underbrace{(\partial_x \lambda_t^*) X_t^* \boldsymbol{\pi}_t^{*\top} \boldsymbol{\sigma}(t, \mathbf{Y}_t^*)}_{\text{Term from } V_{XX} dX_t} + \underbrace{(\partial_{\mathbf{Y}} \lambda_t^*) \boldsymbol{\sigma}_Y(t, \mathbf{Y}_t^*) \rho^\top \Psi^{-1}}_{\text{Term from } V_{X\mathbf{Y}} dY_t \text{ via correlation}}. \quad (17)$$

The first term reflects the direct impact of wealth volatility related to the portfolio choice $\boldsymbol{\pi}_t^*$, scaled by the second derivative of the value function with respect to wealth, V_{XX} (or $\partial_x \lambda_t^*$). The second term captures the intertemporal hedging component arising from the correlation between asset returns and state variable movements, mediated by the cross-derivative of the value function $V_{X\mathbf{Y}}$ (or $\partial_{\mathbf{Y}} \lambda_t^*$).

This derivation provides the explicit form of the adjoint diffusion coefficient $\mathbf{Z}_t^{\lambda X}$, which is fundamental for understanding the structure of the optimal portfolio policy (11) and for constructing the Pontryagin adjoint equations.

B Analytic Solutions for Affine Models

This appendix provides details on the derivation of analytic solutions for the portfolio optimization problems presented in Section 2.3 under specific assumptions (no intermediate consumption, CRRA utility), typically following the Hamilton-Jacobi-Bellman (HJB) approach with an exponential-quadratic value function ansatz. We also show how these solutions connect to the Pontryagin framework.

B.1 Analytic Solution for the Multi-Asset OU Model (Section 2.3.1)

For simplicity, we assume no intermediate consumption, i.e., $C_t = 0$, and consider an investor who derives utility only from terminal wealth X_T under a CRRA objective $U(x) = \frac{x^{1-\gamma}}{1-\gamma}$. Following Kim and Omberg (1996), the associated Hamilton-Jacobi-Bellman (HJB) equation can be solved by positing a value function of the form:

$$V(t, x, Y) = \frac{x^{1-\gamma}}{1-\gamma} \exp\left(g(t) + B(t)Y + \frac{1}{2}C(t)Y^2\right). \quad (18)$$

Here, $g(t)$, $B(t)$, and $C(t)$ are deterministic functions of time determined by solving a system of ordinary differential equations (ODEs) derived from the HJB equation, subject to terminal conditions at $t = T$.

From this value function, the costate $\lambda_t^* = V_x$, its derivative with respect to wealth $\partial_x \lambda_t^* = V_{xx}$, and its derivative with respect to the state $\partial_Y \lambda_t^* = V_{xY}$ have the following closed-form expressions on the optimal path (X_t^*, Y_t) :

$$\begin{aligned}\lambda_t^*(t, X_t^*, Y_t) &= (X_t^*)^{-\gamma} \exp\left(g(t) + B(t)Y_t + \frac{1}{2}C(t)Y_t^2\right), \\ \frac{\partial \lambda_t^*}{\partial x}(t, X_t^*, Y_t) &= -\gamma(X_t^*)^{-\gamma-1} \exp\left(g(t) + B(t)Y_t + \frac{1}{2}C(t)Y_t^2\right), \\ \frac{\partial \lambda_t^*}{\partial Y}(t, X_t^*, Y_t) &= (X_t^*)^{-\gamma} (B(t) + C(t)Y_t) \exp\left(g(t) + B(t)Y_t + \frac{1}{2}C(t)Y_t^2\right).\end{aligned}$$

These expressions lead to remarkably simple ratios that are central to the Pontryagin framework's characterization of the optimal portfolio:

$$\frac{\lambda_t^*}{\partial_x \lambda_t^*} = -\frac{X_t^*}{\gamma}, \quad \frac{\partial_Y \lambda_t^*}{\partial_x \lambda_t^*} = -\frac{X_t^*}{\gamma} (B(t) + C(t)Y_t).$$

Substituting these ratios into the general Pontryagin first-order condition for the optimal portfolio π_t^* (which equates the marginal contribution to the Hamiltonian from investing in risky assets to zero, cf. Eq. (10) derived in Section 2.2) confirms the explicit analytic solution derived via the HJB approach:

$$\pi^*(t, Y) = \frac{1}{\gamma} \Sigma^{-1} \left[\underbrace{(\boldsymbol{\alpha} \boldsymbol{\sigma}) Y}_{\text{Myopic}} + \underbrace{\sigma_Y (\boldsymbol{\sigma} \boldsymbol{\rho}) (B(t) + C(t) Y)}_{\text{Hedging}} \right],$$

where $\Sigma = \text{diag}(\boldsymbol{\sigma}) \Psi \text{diag}(\boldsymbol{\sigma})$, $\boldsymbol{\alpha} = (\alpha_1, \dots, \alpha_n)^\top$, $\boldsymbol{\rho} = (\rho_1, \dots, \rho_n)^\top$, $(\boldsymbol{\alpha} \boldsymbol{\sigma})$ is the vector $(\alpha_1 \sigma_1, \dots, \alpha_n \sigma_n)^\top$, and $(\boldsymbol{\sigma} \boldsymbol{\rho})$ is the vector $(\sigma_1 \rho_1, \dots, \sigma_n \rho_n)^\top$. The derivation confirms that the first term captures the myopic demand driven by the instantaneous risk premium $(\boldsymbol{\mu}(Y) - r\mathbf{1}) = (\boldsymbol{\alpha} \boldsymbol{\sigma}) Y$, while the second term represents the intertemporal hedging demand, proportional to $B(t) + C(t)Y$ which arises from the state-dependency of the investment opportunity set captured by $\partial_Y \lambda_t^*$.

Substituting this π^* back into the HJB equation and matching coefficients in powers of Y yields the following Riccati-type ODEs for $B(t)$ and $C(t)$, along with the ODE for $g(t)$. The system is solved backward from the terminal conditions:

$$g(T) = 0, \quad B(T) = 0, \quad C(T) = 0. \quad (19)$$

The ODEs are:

$$-\frac{dC(t)}{dt} = -2\kappa_Y C(t) + \sigma_Y^2 C(t)^2 + \frac{1-\gamma}{\gamma} \left[\beta_0 + 2\sigma_Y C(t) \beta_1 + \sigma_Y^2 C(t)^2 \beta_2 \right], \quad (20)$$

$$-\frac{dB(t)}{dt} = -\kappa_Y B(t) + \sigma_Y^2 B(t) C(t) - \frac{1-\gamma}{\gamma} \left[\sigma_Y^2 B(t) C(t) \beta_2 + \sigma_Y B(t) \beta_1 \right] + \kappa_Y \theta_Y C(t), \quad (21)$$

$$\frac{dg(t)}{dt} = (1-\gamma)r - \frac{1-\gamma}{2\gamma} \left[\beta_0 + 2\sigma_Y \beta_1 B(t) + \sigma_Y^2 \beta_2 (B(t)^2 + C(t)) \right] + \kappa_Y \theta_Y B(t) + \frac{1}{2} \sigma_Y^2 C(t). \quad (22)$$

Here, r is the risk-free rate, κ_Y , θ_Y , σ_Y are the OU parameters, γ is the risk aversion coefficient, and β_0 , β_1 , β_2 are quadratic forms involving the model parameters defined as:

$$\beta_0 := (\boldsymbol{\alpha} \boldsymbol{\sigma})^\top \Sigma^{-1} (\boldsymbol{\alpha} \boldsymbol{\sigma}), \quad \beta_1 := (\boldsymbol{\alpha} \boldsymbol{\sigma})^\top \Sigma^{-1} (\boldsymbol{\sigma} \boldsymbol{\rho}), \quad \beta_2 := (\boldsymbol{\sigma} \boldsymbol{\rho})^\top \Sigma^{-1} (\boldsymbol{\sigma} \boldsymbol{\rho}).$$

By solving the system of ODEs (20), (21), and (22) backward in time from the terminal conditions (19), one obtains the functions $g(t)$, $B(t)$, and $C(t)$. Substituting these into Eq. (18) gives the complete analytic form of the value function consistent with the underlying HJB/PMP framework.

B.2 Analytic Solution for the Multi-Asset Multi-Factor Model (Section 2.3.2)

For simplicity, we again assume no intermediate consumption ($C_t = 0$) and focus on an investor who maximizes the expected utility of terminal wealth under CRRA utility $U(x) = \frac{x^{1-\gamma}}{1-\gamma}$. Following related literature on multi-factor affine models, we posit a value function of the form

$$V(t, x, \mathbf{Y}) = \frac{x^{1-\gamma}}{1-\gamma} \exp\left\{g(t) + \mathbf{B}(t)^\top \mathbf{Y} + \frac{1}{2} \mathbf{Y}^\top \mathbf{C}(t) \mathbf{Y}\right\}, \quad (23)$$

where $\mathbf{B}(t)$ is an $k \times 1$ vector, $\mathbf{C}(t)$ is an $k \times k$ symmetric matrix (note: dimensions based on state vector $\mathbf{Y} \in \mathbb{R}^k$), and $g(t)$ is a scalar function, all satisfying ODEs derived from the HJB equation, with terminal conditions $g(T) = 0$, $\mathbf{B}(T) = \mathbf{0}$ and $\mathbf{C}(T) = \mathbf{0}$.

Define the relevant matrices and vectors:

$$\boldsymbol{\sigma} = \text{diag}(\sigma_1, \dots, \sigma_n), \quad \boldsymbol{\sigma}_Y \text{ (factor diffusion } k \times k), \quad \Sigma = \boldsymbol{\sigma} \Psi \boldsymbol{\sigma}.$$

where $\Psi \in \mathbb{R}^{n \times n}$ is the correlation matrix for the n risky assets, and let $\rho \in \mathbb{R}^{n \times k}$ be the cross-correlation matrix between these assets and the k -dimensional factor Brownian motion \mathbf{W}_t^Y . Also let $\mathbf{A} = (\boldsymbol{\alpha}_1, \dots, \boldsymbol{\alpha}_n)^\top \in \mathbb{R}^{n \times k}$ collect the factor loadings $\boldsymbol{\alpha}_i \in \mathbb{R}^k$ for each asset i .

The costate $\lambda_t^* = V_x$, its derivative with respect to wealth $\partial_x \lambda_t^* = V_{xx}$, and its gradient ($k \times 1$ vector) with respect to the state vector $\partial_{\mathbf{Y}} \lambda_t^* = V_{x\mathbf{Y}}$ are given by:

$$\begin{aligned} \lambda_t^*(t, X_t^*, \mathbf{Y}_t) &= (X_t^*)^{-\gamma} \exp\left(g(t) + \mathbf{B}(t)^\top \mathbf{Y}_t + \frac{1}{2} \mathbf{Y}_t^\top \mathbf{C}(t) \mathbf{Y}_t\right), \\ \frac{\partial \lambda_t^*}{\partial x}(t, X_t^*, \mathbf{Y}_t) &= -\gamma (X_t^*)^{-\gamma-1} \exp\left(g(t) + \mathbf{B}(t)^\top \mathbf{Y}_t + \frac{1}{2} \mathbf{Y}_t^\top \mathbf{C}(t) \mathbf{Y}_t\right), \\ \frac{\partial \lambda_t^*}{\partial \mathbf{Y}}(t, X_t^*, \mathbf{Y}_t) &= (X_t^*)^{-\gamma} (\mathbf{B}(t) + \mathbf{C}(t) \mathbf{Y}_t) \exp\left(g(t) + \mathbf{B}(t)^\top \mathbf{Y}_t + \frac{1}{2} \mathbf{Y}_t^\top \mathbf{C}(t) \mathbf{Y}_t\right). \end{aligned}$$

These yield the following scalar and vector ratios, which simplify the PMP optimality conditions:

$$\frac{\lambda_t^*}{\partial_x \lambda_t^*} = -\frac{X_t^*}{\gamma}, \quad \frac{\partial_{\mathbf{Y}} \lambda_t^*}{\partial_x \lambda_t^*} = -\frac{X_t^*}{\gamma} (\mathbf{B}(t) + \mathbf{C}(t) \mathbf{Y}_t).$$

Substituting these into the vector form of the PMP first-order condition for the optimal portfolio $\boldsymbol{\pi}_t^* \in \mathbb{R}^n$, (cf. Eq. (11) derived in Section 2.2):

$$\boldsymbol{\pi}_t^* = -\frac{1}{X_t^* \partial_x \lambda_t^*} \Sigma^{-1} \left\{ \lambda_t^* (\boldsymbol{\mu}(\mathbf{Y}_t) - r\mathbf{1}) + \boldsymbol{\sigma} \rho \boldsymbol{\sigma}_Y \left[(\partial_{\mathbf{Y}} \lambda_t^*)^\top \right] \right\},$$

where the risk premium vector is $\boldsymbol{\mu}(\mathbf{Y}_t) - r\mathbf{1} = \boldsymbol{\sigma} \mathbf{A} \mathbf{Y}_t$, we precisely recover the analytic solution obtained from the HJB framework:

$$\boldsymbol{\pi}^*(t, \mathbf{Y}) = \frac{1}{\gamma} \Sigma^{-1} \left[\underbrace{\boldsymbol{\sigma} \mathbf{A} \mathbf{Y}}_{\text{Myopic component (related to } \boldsymbol{\mu} - r\mathbf{1})}} + \underbrace{\boldsymbol{\sigma} \rho \boldsymbol{\sigma}_Y (\mathbf{B}(t) + \mathbf{C}(t) \mathbf{Y})}_{\text{Hedging component (related to } \partial_{\mathbf{Y}} \lambda_t^*)} \right].$$

Here, the first bracketed term corresponds to the *myopic* component, driven by the instantaneous expected excess returns $\boldsymbol{\sigma} \mathbf{A} \mathbf{Y}$. The second bracketed term incorporates *intertemporal hedging* demands arising from the desire to hedge against unfavorable changes in the investment opportunity set, as captured by the factor sensitivities $\mathbf{B}(t) + \mathbf{C}(t) \mathbf{Y}$ (proportional to the

gradient $\partial_{\mathbf{Y}} \lambda_t^*$) and the correlations encoded in ρ , Ψ , and Φ (implicitly via the ODEs for \mathbf{B} and \mathbf{C}).

To determine the time-dependent coefficients $\mathbf{B}(t)$ and $\mathbf{C}(t)$, we solve the backward matrix Riccati ODE system derived from substituting the value function ansatz and optimal portfolio into the HJB equation:

$$\begin{aligned} \frac{d\mathbf{C}(t)}{dt} &= \kappa_Y^\top \mathbf{C}(t) + \mathbf{C}(t) \kappa_Y - \mathbf{C}(t) \boldsymbol{\sigma}_Y \Phi \boldsymbol{\sigma}_Y^\top \mathbf{C}(t) \\ &\quad - \frac{1-\gamma}{\gamma} \left[(\mathbf{A}^\top \boldsymbol{\sigma}) \Sigma^{-1} (\boldsymbol{\sigma} \mathbf{A}) + (\mathbf{A}^\top \boldsymbol{\sigma}) \Sigma^{-1} (\boldsymbol{\sigma} \rho \boldsymbol{\sigma}_Y) \mathbf{C}(t) \right. \\ &\quad \left. + \mathbf{C}(t) (\boldsymbol{\sigma}_Y^\top \rho^\top \boldsymbol{\sigma}) \Sigma^{-1} (\boldsymbol{\sigma} \mathbf{A}) + \mathbf{C}(t) (\boldsymbol{\sigma}_Y^\top \rho^\top \boldsymbol{\sigma}) \Sigma^{-1} (\boldsymbol{\sigma} \rho \boldsymbol{\sigma}_Y) \mathbf{C}(t) \right], \end{aligned} \quad (24)$$

$$\begin{aligned} \frac{d\mathbf{B}(t)}{dt} &= \left[\kappa_Y^\top - \mathbf{C}(t) \boldsymbol{\sigma}_Y \Phi \boldsymbol{\sigma}_Y^\top - \frac{1-\gamma}{\gamma} \left(\mathbf{C}(t) (\boldsymbol{\sigma}_Y^\top \rho^\top \boldsymbol{\sigma}) \Sigma^{-1} (\boldsymbol{\sigma} \rho \boldsymbol{\sigma}_Y) + (\mathbf{A}^\top \boldsymbol{\sigma}) \Sigma^{-1} (\boldsymbol{\sigma} \rho \boldsymbol{\sigma}_Y) \right) \right] \mathbf{B}(t) \\ &\quad - \left[\mathbf{C}(t) \kappa_Y - \frac{1-\gamma}{\gamma} (\mathbf{A}^\top \boldsymbol{\sigma}) \Sigma^{-1} (\boldsymbol{\sigma} \mathbf{A}) \right] \boldsymbol{\theta}_Y. \end{aligned} \quad (25)$$

subject to the terminal conditions $\mathbf{C}(T) = \mathbf{0}$ and $\mathbf{B}(T) = \mathbf{0}$.

To obtain the complete value function (23), the scalar function $g(t)$ must also be determined by solving its own ODE backward from the terminal condition $g(T) = 0$. This ODE, derived from the HJB equation by collecting terms independent of \mathbf{Y} and consistent with the corrected single-factor case structure, is given by:

$$\begin{aligned} \frac{dg(t)}{dt} &= (1-\gamma)r \\ &\quad - \frac{1-\gamma}{2\gamma} \text{Tr} \left((\mathbf{A}^\top \boldsymbol{\sigma}) \Sigma^{-1} (\boldsymbol{\sigma} \mathbf{A}) \right) \\ &\quad - \frac{1-\gamma}{\gamma} \mathbf{B}(t)^\top (\boldsymbol{\sigma}_Y^\top \rho^\top \boldsymbol{\sigma}) \Sigma^{-1} (\boldsymbol{\sigma} \mathbf{A}) \\ &\quad - \frac{1-\gamma}{2\gamma} \left[\mathbf{B}(t)^\top (\boldsymbol{\sigma}_Y^\top \rho^\top \boldsymbol{\sigma}) \Sigma^{-1} (\boldsymbol{\sigma} \rho \boldsymbol{\sigma}_Y) \mathbf{B}(t) + \text{Tr} \left((\boldsymbol{\sigma}_Y^\top \rho^\top \boldsymbol{\sigma}) \Sigma^{-1} (\boldsymbol{\sigma} \rho \boldsymbol{\sigma}_Y) \mathbf{C}(t) \right) \right] \\ &\quad + \mathbf{B}(t)^\top \kappa_Y \boldsymbol{\theta}_Y \\ &\quad + \frac{1}{2} \text{Tr} (\mathbf{C}(t) \boldsymbol{\sigma}_Y \Phi \boldsymbol{\sigma}_Y^\top). \end{aligned} \quad (26)$$

Here, $\Phi = \text{Cov}(d\mathbf{W}_t^Y)/dt$ is the factor covariance matrix used in the factor dynamics $d\mathbf{Y}_t$, and $\text{Tr}(\cdot)$ denotes the trace of a matrix.

Solving these coupled ODEs for $\mathbf{C}(t)$, $\mathbf{B}(t)$, and $g(t)$ backward in time from T to t and substituting the results into Eq. (23) gives the closed-form value function, while substituting $\mathbf{B}(t)$ and $\mathbf{C}(t)$ into $\boldsymbol{\pi}^*(t, \mathbf{Y})$ gives the optimal strategy, explicitly capturing both *myopic* and *intertemporal hedging* components in a multi-asset, multi-factor setting.

C Detailed Proofs for the Policy Gap Bound (Theorem 1) and Supporting Results

This appendix provides the detailed mathematical arguments supporting the Policy Gap Bound stated in Theorem 1 (see Section 3.3). These details include the precise statements of the necessary assumptions (Assumptions 6 and 7), and the full proof sketches for the lemmas, propositions, and Theorem 4 that collectively establish the theoretical justification for the Projected PG-DPO approach. The core result demonstrates that if the policy (π, c) obtained from the Stage 1 warm-up phase satisfies a sufficiently small Pontryagin first-order condition (FOC) residual ε , then the feedback policy $\hat{\pi}$ constructed in Stage 2 using BPTT estimates $\hat{\lambda}$ (with error δ_{BPTT}) will be close to the true optimal policy π^* .

Objective and Roadmap. This section provides the mathematical justification for the Projected PG-DPO approach. We establish that if the policy (π, c) obtained from the Stage 1 warm-up phase satisfies a sufficiently small Pontryagin first-order condition (FOC) residual ε , then the feedback policy $\hat{\pi}$ constructed in Stage 2 using BPTT estimates $\hat{\lambda}$ (with error δ_{BPTT}) will be close to the true optimal policy π^* . Our proof follows the logical chain:

$$\text{FOC-gap}(\leq \varepsilon) \implies \text{Coupled Gaps } (E_f, E_h, E_v \text{ are } O(\varepsilon)) \implies \text{Policy-gap } (\leq O(\varepsilon + \delta_{\text{BPTT}})).$$

The core involves establishing bounds via lemmas and propositions, resolving coupled estimates, and concluding with the main theorem.

1. Preliminaries: PDE, Norms, and Regularity. We work within the framework established in Section 2. For any admissible policy (π, c) , the associated sub-value function $V^{\pi, c}$ solves the linear parabolic PDE:

$$-\partial_t V^{\pi, c} = \mathcal{L}_{\pi, c}[V^{\pi, c}] + f_{\pi, c}, \quad V^{\pi, c}(T, z) = g(z), \quad (27)$$

where the operator $\mathcal{L}_{\pi, c}$ and source term $f_{\pi, c}$ depend on the policy (π, c) . This dependence occurs through specific functions determining the PDE coefficients and the source term. For the purpose of tracking policy influence in our analysis, we conceptually group the key policy-dependent components under the label (C) below :

- **Wealth Drift Influence:** Terms multiplying V_x dependent on π_t, C_t .
- **Wealth Diffusion Influence:** Term multiplying V_{xx} dependent on π_t .
- **Wealth-State Cross-Diffusion Influence:** Terms multiplying V_{xy_j} dependent on π_t .
- **Consumption Source Term:** $f_{\pi, c} = e^{-\delta t} U(C_t)$.

We use standard mixed $L^{q,p}(Q_T)$ space-time norms over the domain $Q_T = (0, T) \times \Omega$, where $\Omega \subseteq \mathbb{R}^d$ is the spatial domain, with $p > d + 2$ and $q \geq 2$. We define the error norms: $E_f = \|f_{\pi^*, c^*} - f_{\pi, c}\|_{L^{q,p}}$, $E_h = \|h\|_{L^{q,p}}$ (where h represents the difference in policy influence on PDE coefficients as per (C)), and $E_v = \|\nabla V^{\pi^*, c^*} - \nabla V^{\pi, c}\|_{L^{q,p}}$.

2. Standing Assumptions. Our analysis relies on standard regularity conditions.

Assumption 6 (Parabolic Regularity). *We assume: (a) The maps from policy (π, c) to PDE coefficients (drift b , diffusion a) are Lipschitz continuous with constant L_{coef} . (b) The Hamiltonian $H(t, z, V, X, \pi, c)$ is C^2 in its arguments; its gradient $\nabla_{(\pi, c)} H$ is Lipschitz continuous in $X := \nabla V$ with constant L_{HX} . (c) The map from costates to controls via PMP FOCs, $F : (\lambda, \nabla \lambda) \mapsto (\pi, c)$, is locally Lipschitz. Standard uniform parabolicity holds: $\xi^\top a(t, z, \pi, c) \xi \geq \underline{\nu} \|\xi\|^2$ for some $\underline{\nu} > 0$. Coefficients are sufficiently smooth for PDE regularity results (e.g., VMO in space, bounded measurable in time).*

Assumption 7 (FOC Gap). *The policy (π, c) from Stage 1 and its costate $\lambda = \nabla V^{\pi, c}$ satisfy:*

$$\|\mathcal{R}_{\text{FOC}}(\pi, c; \lambda)\|_{L^{q,p}} \leq \varepsilon,$$

where $\mathcal{R}_{\text{FOC}} := \nabla_{(\pi, c)} H(t, z, V^{\pi, c}, \nabla V^{\pi, c}, \pi, c)$.

3. Key Technical Results.

Lemma 2 (FOC-reduction: coefficient-gap bound, full version). *Let Assumptions 6–7 hold and assume further that*

$$\exists \underline{\Lambda} > 0 : \quad -\nabla_{(\pi, c)}^2 H \succeq \underline{\Lambda} I_{(n+1) \times (n+1)} \quad \text{for all } (t, z, \pi, c) \text{ in the admissible set } \mathcal{A}, \quad (28)$$

i.e. the Hamiltonian is uniformly strongly concave in the control variables. Let $h(t, z)$ collect the differences of every coefficient (in drift, diffusion and cross terms) of the linear operator $\mathcal{L}_{\pi, c}$ when (π, c) is substituted for the optimal control (π^*, c^*) . Then, for all $(t, z) \in (0, T) \times \Omega$,

$$|h(t, z)| \leq L_H |\nabla V^{\pi, c}(t, z) - \nabla V^*(t, z)| + C_{\text{FOC}} |\mathcal{R}_{\text{FOC}}(t, z)|, \quad (29)$$

with finite constants

$$L_H := L_{\text{coef}} \frac{L_{HX}}{\underline{\Lambda}}, \quad C_{\text{FOC}} := L_{\text{coef}} \frac{1}{\underline{\Lambda}}, \quad (30)$$

where L_{coef} and L_{HX} are as defined in Assumption 6. (Dependence: L_H, C_{FOC} depend only on $\underline{\Lambda}, L_{\text{coef}}, L_{HX}$ and therefore ultimately on the model parameters fixed in Assumption 6.)

Proof. First, we define the implicit system $F(\pi, c; V, X) := \nabla_{(\pi, c)} H(t, z, V, X, \pi, c)$, where $X := \nabla V$. For every fixed state point (t, z) , the first-order condition is $F(\pi, c; V, X) = 0$. The optimal pair (π^*, c^*) satisfies $F(\pi^*, c^*; V^*, \nabla V^*) = 0$.

Next, by the uniform strong concavity (28), $\nabla_{(\pi, c)} F = -\nabla_{(\pi, c)}^2 H$ is invertible on \mathcal{A} and $\|(\nabla_{(\pi, c)} F)^{-1}\| \leq \underline{\Lambda}^{-1}$. Hence, the Implicit-Function Theorem yields a C^1 -map $\Phi : (V, X) \mapsto (\pi, c)$ on a neighbourhood of (V^*, X^*) with $\|\nabla \Phi(V, X)\| = \|(\nabla_{(\pi, c)} F)^{-1} \nabla_{(V, X)} F\| \leq \underline{\Lambda}^{-1} L_{HX} =: C_H$ for all (V, X) in the neighbourhood.

Then, we establish a mean-value bound for the control gap. For the non-optimal pair (π, c) , we have $(\pi, c) - (\pi^*, c^*) = \Phi(V^{\pi, c}, \nabla V^{\pi, c}) - \Phi(V^*, \nabla V^*)$. By the mean-value theorem in Banach spaces, $|(\pi, c) - (\pi^*, c^*)| \leq C_H |\nabla V^{\pi, c} - \nabla V^*| + \underline{\Lambda}^{-1} |F(\pi, c; V^{\pi, c}, \nabla V^{\pi, c})|$. The second term equals $|\mathcal{R}_{\text{FOC}}|$ by Assumption 7.

Finally, we translate this to a coefficient gap. Because the mapping $(\pi, c) \mapsto (b, a)$ (PDE coefficients) is L_{coef} -Lipschitz (Assumption 6(a)), $|h(t, z)| \leq L_{\text{coef}} |(\pi, c) - (\pi^*, c^*)|$. Substituting the estimate from the previous paragraph gives $|h| \leq L_{\text{coef}} C_H |\nabla V - \nabla V^*| + L_{\text{coef}} \underline{\Lambda}^{-1} |\mathcal{R}_{\text{FOC}}|$. The stated constants L_H, C_{FOC} now follow by definition. \square

Lemma 3 (Source-gap bound, full version). *Fix $p > d + 2$, $q \geq 2$ and let the standing assumptions 6–7 hold. Assume furthermore that there exist deterministic constants*

$$0 < \underline{c} < \bar{c} < \infty, \quad 0 < \underline{\lambda} < \bar{\lambda} < \infty, \quad (31)$$

such that for every admissible trajectory and for a.e. $t \in [0, T]$

$$\underline{c} \leq c_t, \quad c_t^* \leq \bar{c}, \quad \underline{\lambda} \leq \lambda_t, \quad \lambda_t^* \leq \bar{\lambda},$$

where $\lambda_t := V_x^{\pi, c}(t, \cdot)$ and $\lambda_t^* := V_x^*(t, \cdot)$. Let

$$E_f := \|e^{-\delta t} (U(c^*) - U(c))\|_{L^{q, p}}, \quad E_v := \|\nabla V^* - \nabla V^{\pi, c}\|_{L^{q, p}},$$

and write $\varepsilon := \|\mathcal{R}_{\text{FOC}}\|_{L^{q, p}}$ for the first-order-condition residual norm. Then

$$E_f \leq C_f \varepsilon + C'_f E_v, \quad (32)$$

with explicit finite constants

$$C_f = \bar{c}^{-\gamma} L_{(U')^{-1}}, \quad C'_f = L_{(U')^{-1}}, \quad L_{(U')^{-1}} = \frac{\bar{\lambda}^{\frac{\gamma+1}{\gamma}}}{\gamma} \underline{c}^\gamma. \quad (33)$$

(All dependence on the model is through $\delta, \gamma, \underline{c}, \bar{c}, \underline{\lambda}, \bar{\lambda}$.)

Proof. Throughout the proof, we abbreviate $\|\cdot\|_{q,p} := \|\cdot\|_{L^{q,p}}$. For CRRA utility $U(c) = c^{1-\gamma}/(1-\gamma)$ with $\gamma > 1$, we have $U'(c) = c^{-\gamma}$ and $(U')^{-1}(\ell) = \ell^{-1/\gamma}$. By (31), $\sup_{c \in [\underline{c}, \bar{c}]} U'(c) = \underline{c}^{-\gamma} < \infty$, and $\sup_{\ell \in [\underline{\lambda}, \bar{\lambda}]} |(U')^{-1}(\ell)| = \frac{1}{\gamma} \underline{c}^\gamma \bar{\lambda}^{\frac{\gamma+1}{\gamma}} =: L_{(U')^{-1}}$. Hence $(U')^{-1}$ is globally Lipschitz on $[\underline{\lambda}, \bar{\lambda}]$ with constant $L_{(U')^{-1}}$.

Next, by Taylor expansion of U , for every (t, ω) there exists $c_{t,\omega}^\dagger \in [\underline{c}, \bar{c}]$ such that $U(c_t^*) - U(c_t) = U'(c_{t,\omega}^\dagger)(c_t^* - c_t)$, and $|U'(c_{t,\omega}^\dagger)| \leq \underline{c}^{-\gamma}$. Multiplying by $e^{-\delta t}$ and taking absolute values yields $e^{-\delta t} |U(c_t^*) - U(c_t)| \leq \underline{c}^{-\gamma} e^{-\delta t} |c_t^* - c_t|$.

Furthermore, the first-order condition for consumption gives $e^{-\delta t} U'(c_t^*) = \lambda_t^*$ and $e^{-\delta t} U'(c_t) = \lambda_t - \mathcal{R}_{\text{FOC}}^{(c)}(t)$, where $\mathcal{R}_{\text{FOC}}^{(c)}$ denotes the consumption component of the FOC-residual. Because both arguments $\ell^* := \lambda_t^*$ and $\ell := \lambda_t - \mathcal{R}_{\text{FOC}}^{(c)}(t)$ lie in $[\underline{\lambda}, \bar{\lambda}]$, the Lipschitz property of $(U')^{-1}$ yields $|c_t^* - c_t| \leq L_{(U')^{-1}} (|\lambda_t - \lambda_t^*| + |\mathcal{R}_{\text{FOC}}^{(c)}(t)|)$.

Combining these results, we insert the bound for $|c_t^* - c_t|$ into the inequality for $e^{-\delta t} |U(c_t^*) - U(c_t)|$ to get $e^{-\delta t} |U(c_t^*) - U(c_t)| \leq \left(\underline{c}^{-\gamma} L_{(U')^{-1}} \right) (|\lambda_t - \lambda_t^*| + |\mathcal{R}_{\text{FOC}}^{(c)}(t)|)$. Taking the $L^{q,p}$ -norm, using the definitions of E_v and ε , and noting $|\lambda - \lambda^*| = |V_x^{\pi,c} - V_x^*| \leq |\nabla V^{\pi,c} - \nabla V^*|$, we conclude $E_f \leq \underline{c}^{-\gamma} L_{(U')^{-1}} \varepsilon + L_{(U')^{-1}} E_v$. With C_f, C_f' chosen as in the statement, (32) follows. \square

Proposition C.1 (Value- and gradient-gap stability, full version). *Fix exponents $p > d+2$, $q \geq 2$. Under Assumption 6 (coefficient regularity, uniform parabolicity) and with the notation*

$$E_f := \|f\|_{L^{q,p}}, \quad E_h := \|h\|_{L^{q,p}}, \quad E_v := \|\nabla V^{\pi,c} - \nabla V^*\|_{L^{q,p}},$$

one has

$$E_v \leq C_S (E_f + E_h), \tag{34}$$

where the stability constant C_S depends only on $p, q, T, d, \underline{\nu}, \|a^*\|_{L^\infty}, \|b^*\|_{L^\infty}$ ($\underline{\nu}$: the uniform ellipticity constant; a^*, b^* : diffusion and drift coefficients of \mathcal{L}_{π^*, c^*}).

Proof. First, we consider the equation for the difference $W := V^{\pi,c} - V^*$. Recall that, for each admissible control, $V^{\pi,c}$ solves the linear backward parabolic PDE $-\partial_t V^{\pi,c} + \mathcal{L}_{\pi,c} V^{\pi,c} = f_{\pi,c}$, with $V^{\pi,c}(T, \cdot) = g$, where the terminal datum is $g(x) = \kappa U(x)$. Subtracting the optimal-control equation yields $-\partial_t W + \mathcal{L}_* W = f + h \cdot \nabla V^{\pi,c}$, with $W(T, \cdot) = 0$. Here $\mathcal{L}_* := \mathcal{L}_{\pi^*, c^*}$, $f := f_{\pi,c} - f_{\pi^*, c^*}$, and $h := (b_{\pi,c} - b_*, a_{\pi,c} - a_*)$ abbreviates the vector of coefficient gaps; thus $h \in L^{q,p}$ by Lemma 2.

Regarding the coefficient class, Assumption 6(a) implies that $(t, x) \mapsto a_*(t, x)$ is uniformly VMO in x with bounded measurable t -dependence, and satisfies the ellipticity bound $\underline{\nu} |\xi|^2 \leq \xi^\top a_*(t, x) \xi \leq \|a_*\|_\infty |\xi|^2$. The lower order coefficients b_* are bounded.

For the source term, define $g_{src} := f + h \cdot \nabla V^{\pi,c}$ (using g_{src} to avoid conflict with terminal data g). By Lemma 3 and Lemma 2, $f, h \in L^{q,p}$. Moreover, $\nabla V^{\pi,c} \in L^{q,p}$ (by maximal-regularity for $V^{\pi,c}$), hence $g_{src} \in L^{q,p}$ and $\|g_{src}\|_{q,p} \leq E_f + E_h$.

Then, we obtain an $L^{q,p}$ -gradient estimate. The equation for W is a linear, non-divergence form, backward parabolic PDE with VMO diffusion coefficients, bounded drift, zero terminal data, and right-hand side $g_{src} \in L^{q,p}$. Therefore, Dong–Kim (Dong and Kim, 2009, Thm. 2.1) (adapted to the backward direction by time reversal) yields $\|\nabla W\|_{L^{q,p}} \leq C_{DK} \|g_{src}\|_{L^{q,p}}$, where $C_{DK} = C_{DK}(p, q, d, T, \underline{\nu}, \|a_*\|_\infty, \|b_*\|_\infty)$.

Finally, inserting the bound on g_{src} and setting $C_S := C_{DK}$ leads to the conclusion (34). \square

Proposition C.2 (Coupled error-estimate resolution, full version). *Let the constants $C_f, C_f', L_H, C_{\text{FOC}}, C_S$ be those obtained in Lemmas 3, 2 and Proposition C.1. Define $\rho := C_S(C_f' + L_H)$. Then, under Assumptions 6–7, the error triple (E_f, E_h, E_v) satisfies*

$$E_f \leq C_f'' \varepsilon, \quad E_h \leq C_h'' \varepsilon, \quad E_v \leq C_v'' \varepsilon, \tag{35}$$

with finite constants

$$C_v'' = \frac{C_S(C_f + C_{\text{FOC}})}{1 - \rho_*}, \quad C_f'' = C_f + C_f' C_v'', \quad C_h'' = C_{\text{FOC}} + L_H C_v'',$$

where if $\rho < 1$, we may take $\rho_* := \rho$; otherwise, if $\rho \geq 1$, pick an integer $m \geq 1$ such that $\rho_\Delta := C_S(\Delta)(C_f' + L_H) < 1$ for $\Delta := T/m$ (possible because $C_S(\Delta) \rightarrow 0$ as $\Delta \downarrow 0$). Then set $\rho_* := \rho_\Delta$ and $C_S := \max_{0 \leq k < m} C_S(\Delta)$. (The constants depend on $p, q, T, d, \underline{\nu}, \|a^*\|_\infty, \|b^*\|_\infty$ only through $C_f, C_f', L_H, C_{\text{FOC}}, C_S$.)

Proof. From Lemma 3, Lemma 2, and Proposition C.1, we have the following basic three inequalities:

$$E_f \leq C_f \varepsilon + C_f' E_v, \quad (36a)$$

$$E_h \leq C_{\text{FOC}} \varepsilon + L_H E_v, \quad (36b)$$

$$E_v \leq C_S (E_f + E_h). \quad (36c)$$

Inserting (36a) and (36b) into (36c) yields a single scalar inequality for E_v :

$$E_v \leq C_S \left[(C_f + C_{\text{FOC}}) \varepsilon + (C_f' + L_H) E_v \right] = C_S (C_f + C_{\text{FOC}}) \varepsilon + \rho E_v.$$

Rearranging this gives $(1 - \rho) E_v \leq C_S (C_f + C_{\text{FOC}}) \varepsilon$.

Now, we consider two cases for ρ . If $\rho < 1$, the inequality immediately gives $E_v \leq \frac{C_S(C_f + C_{\text{FOC}})}{1 - \rho} \varepsilon$. Define $C_v'' := \frac{C_S(C_f + C_{\text{FOC}})}{1 - \rho}$. Back-substituting this into (36a) and (36b) yields (35) with the constants stated for the $\rho < 1$ branch, setting $\rho_* := \rho$.

If $\rho \geq 1$, we use a time-slicing argument. Fix $m \in \mathbb{N}$ and set $\Delta := T/m$. Let $E_v^{(k)}$ denote the $L^{q,p}$ -norm of $\nabla V^{\pi,c} - \nabla V^*$ on the slab $Q_k := (T - k\Delta, T - (k-1)\Delta) \times \Omega$. Because the coefficients are effectively frozen on each slab, Proposition C.1 holds with a short-horizon constant $C_S(\Delta)$, which satisfies $C_S(\Delta) \rightarrow 0$ as $\Delta \downarrow 0$ (as the Dong–Kim estimate is local in time). Repeating the derivation for the scalar inequality for E_v on Q_k yields $E_v^{(k)} \leq \rho_\Delta E_v^{(k-1)} + C_S(\Delta)(C_f + C_{\text{FOC}})\varepsilon$, where $\rho_\Delta := C_S(\Delta)(C_f' + L_H)$. We pick m such that $\rho_\Delta < 1$. Iterating for $k = 1, \dots, m$ and noting $E_v^{(0)} = 0$ (due to the terminal condition $W(T, \cdot) = 0$), we get $E_v^{(m)} \leq \frac{C_S(\Delta)(C_f + C_{\text{FOC}})}{1 - \rho_\Delta} \varepsilon$.

With $C_v'' := \frac{C_S(\Delta)(C_f + C_{\text{FOC}})}{1 - \rho_\Delta}$, $\rho_* := \rho_\Delta$, and C_S redefined as $\max_{0 \leq k < m} C_S(\Delta)$ for the overall bound, the results (35) follow similarly to the $\rho < 1$ case.

In both scenarios, all quantities $C_f, C_f', L_H, C_{\text{FOC}}, C_S(\Delta)$ depend only on the data in Assumption 6. In particular, $C_S(\Delta) \leq C_S(T)$, so C_v'', C_f'', C_h'' are finite. \square

Theorem 4 (Policy Gap Bound). *Under Assumptions 6 and 7, let (π, c) be the policy from Stage 1 satisfying the FOC-gap condition $\|\mathcal{R}_{\text{FOC}}(\pi, c; \lambda)\|_{L^{q,p}} \leq \varepsilon$, where $\lambda = \nabla V^{\pi,c}$. Let π^* be the true optimal policy, and let $\hat{\pi} = F(\hat{\lambda})$ be the policy deployed in Stage 2 using BPTT estimates $\hat{\lambda}$, where F is the explicit mapping from costates $(\lambda, \nabla \lambda)$ to controls derived from the PMP FOCs. Assume F is locally Lipschitz continuous with constant C_F (guaranteed under Assumption 6(c)). If the BPTT estimation error relative to the Stage 1 costate satisfies $\|\hat{\lambda} - \lambda\|_{L^{q,p}} \leq \delta_{\text{BPTT}}$, then the policy gap is bounded by:*

$$\|\hat{\pi} - \pi^*\|_{L^{q,p}} \leq C_{\text{tot}}(\delta_{\text{BPTT}} + \varepsilon)$$

Here, C_{tot} depends on C_F and the constant C_v'' from Proposition C.2.

Proof (detailed). Let (λ_{S1}, Z_{S1}) denote the adapted solution (specifically, $\lambda_{S1} = \nabla V^{\pi,c}$) associated with the Stage 1 policy (π, c) . The BPTT process yields estimates $\hat{\lambda}$ (and implicitly \hat{Z}) for the costate and its related processes. The first-order map $F : (\lambda, \nabla \lambda) \mapsto (\pi, c)$ is C^1 on

a neighbourhood \mathcal{N} of $(\lambda^*, \nabla \lambda^*)$ with Lipschitz constant $\|F\|_{\text{Lip}} \leq C_F := \underline{\Lambda}^{-1} L_{HX}$ (derived similarly to reasoning in Lemma 2, under Assumption 6(c)).

The policy deployed in Stage 2 is $\hat{\pi} = F(\hat{\lambda})$, and the true optimal policy is $\pi^* = F(\nabla V^*)$. We want to bound $\|\hat{\pi} - \pi^*\|_{L^{q,p}}$. Using the Lipschitz continuity of F :

$$\begin{aligned} \|\hat{\pi} - \pi^*\|_{L^{q,p}} &= \|F(\hat{\lambda}) - F(\nabla V^*)\|_{L^{q,p}} \\ &\leq C_F \|\hat{\lambda} - \nabla V^*\|_{L^{q,p}}. \end{aligned}$$

By the triangle inequality,

$$\|\hat{\lambda} - \nabla V^*\|_{L^{q,p}} \leq \|\hat{\lambda} - \lambda_{S1}\|_{L^{q,p}} + \|\lambda_{S1} - \nabla V^*\|_{L^{q,p}}.$$

We are given that the BPTT estimation error $\|\hat{\lambda} - \lambda_{S1}\|_{L^{q,p}} \leq \delta_{\text{BPTT}}$. The term $\|\lambda_{S1} - \nabla V^*\|_{L^{q,p}}$ is precisely $E_v = \|\nabla V^{\pi,c} - \nabla V^*\|_{L^{q,p}}$. From Proposition C.2, we have $E_v \leq C_v'' \varepsilon$. Substituting these into the inequality for $\|\hat{\pi} - \pi^*\|_{L^{q,p}}$:

$$\|\hat{\pi} - \pi^*\|_{L^{q,p}} \leq C_F (\delta_{\text{BPTT}} + E_v) \leq C_F (\delta_{\text{BPTT}} + C_v'' \varepsilon).$$

To express this in the form $C_{\text{tot}}(\delta_{\text{BPTT}} + \varepsilon)$, we can set $C_{\text{tot}} = C_F \max(1, C_v'')$. If $C_v'' \geq 1$, then $C_F(\delta_{\text{BPTT}} + C_v'' \varepsilon) \leq C_F C_v'' (\delta_{\text{BPTT}} + \varepsilon)$. If $C_v'' < 1$, then $C_F(\delta_{\text{BPTT}} + C_v'' \varepsilon) \leq C_F(\delta_{\text{BPTT}} + \varepsilon)$. Thus, $C_{\text{tot}} = C_F \max(1, C_v'')$ provides a valid constant for the boxed expression. Alternatively, one can use $C_{\text{tot}} = C_F(1 + C_v'')$ if one prefers a sum form, as $C_F(\delta_{\text{BPTT}} + C_v'' \varepsilon) \leq C_F(1 + C_v'')(\delta_{\text{BPTT}} + \varepsilon)$ assuming $C_v'' \geq 0$. The choice $C_{\text{tot}} = C_F \max(1, C_v'')$ is tighter. The key result is the linear dependence on δ_{BPTT} and ε . \square

4. Summary and Constant Dependencies. We have demonstrated a clear logical path from a small FOC-gap ε to a small policy gap $O(\varepsilon + \delta_{\text{BPTT}})$, conditional on standard parabolic regularity. The argument relies on establishing key bounds (Lemmas 2, 3), utilizing PDE stability (Proposition C.1), resolving coupled estimates (Proposition C.2), and concluding with the main policy gap theorem (Theorem 4).

It is important to reiterate that all constants ($L_H, C_{\text{FOC}}, C_f, C_f', C_S, C_f'', C_h'', C_v'', C_F, C_{\text{tot}}$) depend quantitatively on model parameters (horizon T , utility U , market coefficients $\boldsymbol{\mu}, \boldsymbol{\sigma}, \dots$), PDE regularity parameters ($p, q, \Omega, \underline{\nu}$), and the costate floor $\underline{\lambda}$. Rigorous derivation requires tracking these dependencies. The provided proofs for lemmas are sketches; full proofs require careful application of MVT, IFT, Taylor expansions, and meticulous handling of bounds. The time-slicing argument mentioned requires careful justification to control constant growth. Subject to these standard technical details, the framework presented provides a sound mathematical basis for the Projected PG-DPO method's effectiveness under the stated regularity conditions.

D Detailed Experimental Setup

This appendix provides the detailed setup for the numerical experiments presented in Section 4.

D.1 Parameter Values

The experiments consider the objective of maximizing the expected utility of terminal wealth X_T , $J = \mathbb{E}[U(X_T)]$, using a CRRA utility function $U(x) = x^{1-\gamma}/(1-\gamma)$ with a relative risk aversion coefficient $\gamma = 2.0$. The fixed time horizon is $T = 1.5$.

Unless otherwise specified, the model parameters (for the model described in Section 2.3.2) are generated based on the asset dimension n and factor dimension k using the following process (seeded for reproducibility, e.g., 'seed=42'):

- Risk-free rate: $r = 0.03$.

- State process parameters (for the k -dimensional OU process \mathbf{Y}_t):
 - Mean-reversion speeds: $\boldsymbol{\kappa}_Y = \text{diag}(2.0, 2.5, \dots, 2.0 + (k - 1)0.5)$.
 - Long-term means: $\boldsymbol{\theta}_Y$ components drawn uniformly from $U(0.2, 0.4)$.
 - Factor volatilities: $\boldsymbol{\sigma}_Y$ diagonal elements drawn uniformly from $U(0.3, 0.5)$.
- Asset parameters (for the n risky assets):
 - Volatilities: $\boldsymbol{\sigma} \in \mathbb{R}^n$ components drawn uniformly from $U(0.1, 0.5)$.
 - Factor loadings ($\boldsymbol{\alpha} \in \mathbb{R}^{n \times k}$): For each asset $i = 1, \dots, n$, the k -dimensional row vector of factor loadings $\boldsymbol{\alpha}_i^\top = (\alpha_{i1}, \dots, \alpha_{ik})$ is drawn independently from a Dirichlet distribution. This is done using ‘scipy.stats.dirichlet’ with a concentration parameter vector consisting of k ones ($\mathbf{1}_k = [1.0, \dots, 1.0]$). Consequently, for each asset i , all loadings are non-negative ($\alpha_{ij} \geq 0$) and they sum to unity ($\sum_{j=1}^k \alpha_{ij} = 1$). (Note: These loadings define the risk premium structure $\boldsymbol{\mu}(t, \mathbf{Y}_t) = r\mathbf{1} + \text{diag}(\boldsymbol{\sigma})\boldsymbol{\alpha}\mathbf{Y}_t$).
- Correlation structure: The generation process aims to produce realistic correlation parameters while ensuring the overall block correlation matrix remains positive definite, which is crucial for stable simulations. This involves:
 - Asset correlation Ψ ($n \times n$) generated based on a latent factor structure ensuring validity.
 - Factor correlation Φ_Y ($k \times k$) generated as a random correlation matrix.
 - Cross-correlation $\boldsymbol{\rho}_Y$ ($n \times k$) components drawn uniformly from $U(-0.2, 0.2)$.
 - The full $(n + k) \times (n + k)$ block correlation matrix $\begin{pmatrix} \Psi & \boldsymbol{\rho}_Y \\ \boldsymbol{\rho}_Y^\top & \Phi_Y \end{pmatrix}$ is constructed and numerically adjusted (e.g., via minimal diagonal loading) if necessary to ensure positive definiteness (tolerance 10^{-6}).

The specific values generated by the seed are used consistently across experiments for given n and k .

D.2 PG-DPO Implementation Details

We implement the Baseline PG-DPO algorithm using PyTorch.

- **Policy Network ($\boldsymbol{\pi}_\theta$):** The policy network architecture consists of an input layer taking the current wealth W_t , current time t , and state vector \mathbf{Y}_t (total $2 + k$ inputs), followed by three hidden layers with 200 units each and LeakyReLU activation, and an output layer producing the n -dimensional portfolio weight vector $\boldsymbol{\pi}_\theta$.
- **Optimizer:** Adam optimizer with a learning rate of 1×10^{-5} .
- **Training:**
 - Total epochs: 10,000.
 - Batch size (M): 1,000.
 - Time discretization steps (N): 20.
 - Initial state sampling (η): For each trajectory in a batch, the initial time t_0 is drawn uniformly from $[0, T)$, initial wealth W_0 from $U(0.1, 3.0)$. The initial state variables $\mathbf{Y}_0 = (Y_{0,1}, \dots, Y_{0,k})^\top$ are sampled such that each component $Y_{0,i}$ is drawn independently and uniformly from a single common range $[Y_{\min}, Y_{\max}]$. This range is

determined by the minimum lower bound and the maximum upper bound observed across all individual factors’ typical $\pm 3\sigma$ intervals:

$$Y_{\min} = \min_{i=1,\dots,k} (\theta_{Y,i} - 3\sigma_{Y,ii}), \quad Y_{\max} = \max_{i=1,\dots,k} (\theta_{Y,i} + 3\sigma_{Y,ii}),$$

where $\theta_{Y,i}$ is the long-term mean and $\sigma_{Y,ii}$ is the instantaneous volatility parameter for the i -th factor. The simulation then runs forward from t_0 to the fixed horizon T using $N = 20$ time steps, with step size $\Delta t = (T - t_0)/N$. This approach ensures the policy is trained effectively across the entire time interval $[0, T]$ and a relevant hypercube in the state space defined by the collective factor dynamics.

- Variance Reduction: Antithetic variates used.
- Wealth constraint: Simulated wealth W_t clamped at lower bound 0.1.
- **Costate Estimation (for Two-Stage Evaluation):** During periodic evaluation, costate λ and derivatives $\partial_x \lambda, \partial_{\mathbf{Y}} \lambda$ are computed via BPTT (`torch.autograd.grad`) applied to Monte Carlo estimates of the expected terminal utility starting from evaluation points (t_k, W_k, \mathbf{Y}_k) .

D.3 Benchmark Solution and Evaluation

As mentioned, the chosen multi-factor OU model allows for a semi-analytical benchmark solution. It is important to note that these experiments focus solely on the terminal wealth objective ($J = \mathbb{E}[U(X_T)]$), and thus do not include optimization or a neural network for the consumption policy C_ϕ . This simplification is made specifically to enable direct comparison with the semi-analytical benchmark solution derived from the HJB equation, which is readily available for the terminal wealth problem in this affine setting.

- **Benchmark Computation:** The system of ODEs (including a matrix Riccati equation) associated with the HJB equation for this terminal wealth problem (Appendix B.2) is solved numerically backwards from the fixed horizon T using `scipy.integrate.solve_ivp` (`‘Radau’` method) to obtain the coefficients determining the value function and the optimal policy $\pi^*(t, W_t, \mathbf{Y}_t)$.
- **Interpolation:** The benchmark policy (total, myopic, and hedging components) is pre-computed on a grid over (t, W_t, \mathbf{Y}_t) space and stored using `scipy.interpolate.RegularGridInterpolator` for efficient lookup.
- **Evaluation Metrics:** Performance is evaluated via the Root Mean Squared Error (RMSE) between the policies generated by (i) Baseline PG-DPO (π_θ) and the benchmark (π^*), and (ii) Two-Stage PG-DPO (using Eq. (11) with BPTT-estimated costates) and the benchmark (π^*). RMSEs are computed for total, myopic, and hedging components.
- **Visualization:** Contour plots compare the learned policies and the benchmark over the state space (typically time t vs. one state variable Y_k), alongside error plots and costate visualizations.

All computations are performed using PyTorch on an NVIDIA A6000 GPU.

D.4 Deep BSDE Implementation Details

The Deep BSDE method, serving as a benchmark, was implemented based on the standard framework by Han et al. (2018) and Weinan (2017). This approach reformulates the problem’s PDE as a backward stochastic differential equation (BSDE) and approximates its solution components using neural networks. Our PyTorch implementation addresses the multi-asset, multi-factor portfolio optimization problem from Section 2.3.2.

- **Network Architectures:** Two main feedforward neural networks with Tanh activations are utilized:
 - **Y0Net:** Approximates the value function at the initial time of a path, $Y_{t_0} \approx V(t_0, X_{t_0}, \mathbf{Y}_{t_0})$. It takes the initial state $(t_0, \log X_{t_0}, \mathbf{Y}_{t_0})$ (total $2 + k$ inputs) as input and produces a scalar output (with a final negative softplus transformation). It typically uses 2 hidden layers of 64 units.
 - **ZNet:** Approximates \mathbf{Z}_t , which relates to the scaled gradient of the value function concerning the underlying Brownian motions, at each time step t . It takes the current state $(t, \log X_t, \mathbf{Y}_t)$ as input and outputs an $(n + k)$ -dimensional vector, representing $\mathbf{Z}_t^X \in \mathbb{R}^n$ and $\mathbf{Z}_t^Y \in \mathbb{R}^k$. It typically uses 3 hidden layers of 128 units.
- **Policy Derivation:** The optimal portfolio $\boldsymbol{\pi}_t$ is dynamically constructed at each step. This involves using the network outputs Y_t (obtained by evolving Y_{t_0} via the BSDE discretization using ZNet) and \mathbf{Z}_t (from ZNet) to approximate the first-order conditions of the HJB equation. This structure allows the policy to learn both myopic demand (from current factor states \mathbf{Y}_t) and intertemporal hedging demand (where terms involving \mathbf{Z}_t^Y/Y_t approximate the necessary factor sensitivities, akin to the analytical solution’s form).
- **Loss Function:** The Y0Net predicts Y_{t_0} . This value, along with ZNet’s outputs for \mathbf{Z}_t , is used to discretize the BSDE forward in time from t_0 to the terminal time T . The training objective is to minimize the mean squared error between the resulting Y_T and the specified terminal utility $U(X_T) = X_T^{1-\gamma}/(1-\gamma)$.
- **Training Details:** The networks are trained for 10,000 epochs using the Adam optimizer (initial learning rate 3×10^{-5} , with a multi-step decay scheduler) and a batch size of 1,024. Each BSDE path is discretized into $N_{\text{BSDE}} = 80$ time steps. Gradient clipping (norm 2.0) and bounding of portfolio weights are applied to enhance training stability.
- **Initial State Sampling:** For each training path, the initial time t_0 is sampled uniformly from the discrete time steps over $[0, T - \Delta t]$. The initial wealth X_0 is drawn uniformly from $[0.1, 3.0]$, and initial factor states \mathbf{Y}_0 are sampled uniformly from a hyperrectangle representing their typical dynamic range (e.g., based on ± 3 stationary standard deviations around their long-term means).

The implementation uses PyTorch and is executed on the same NVIDIA A6000 GPU hardware as the PG-DPO experiments to ensure a fair comparison.